# Evaluation of natural background levels of high mountain karst aquifers in complex hydrogeological settings. A Gaussian mixture model approach in the Port del Comte (SE, Pyrenees) case study

Herms, I.[a], Jódar, J.[b*], Soler, A.[c], Lambán, L.J.[b], Custodio, E.[d], Núñez, J.A.[a], Arnó, G.[a], Ortego, M.I.[e], Parcerisa, D.[f], Jorge, J.[f]

(a) Àrea de Recursos Geològics. Institut Cartogràfic i Geològic de Catalunya (ICGC), Barcelona, Spain
(b) Instituto Geológico Minero de España (IGME), Zaragoza, Spain
(c) Grup MAiMA, SGR Mineralogia Aplicada, Geoquímica i Geomicrobiologia, Departament de Mineralogia, Petrologia i Geologia Aplicada, Facultat de Ciències de la Terra, Universitat de Barcelona (UB), Barcelona, Spain
(d) Spanish Royal Academy of Sciences. Groundwater Hydrogeology Group, Dept. of Civil and Environmental Engineering, Technical University of Catalonia (UPC), Barcelona, Spain
(e) Compositional and Spatial Data Analysis (COSDA) Research Group. Department of Civil and Environmental Engineering, Universitat Politècnica de Catalunya BarcelonaTech, Spain
(f) Departament d'Enginyeria Minera, Industrial i TIC. Universitat Politècnica de Catalunya (UPC), Manresa, Spain
* Corresponding author: j.jodar@igme.es (J.Jódar)

## Abstract

The hydrogeological processes driving the hydrochemical composition of groundwater in the alpine pristine aquifer system of the Port del Comte Massif (PCM) are characterized through the multivariate statistical techniques Principal Component Analysis (PCA) and Gaussian Mixture Models (GMM) in the framework of Compositional Data (CoDa) analysis. Also, the groundwater Natural Background Levels (NBLs) for $NO_3$ and $SO_4$ and Cl are evaluated, which are specially important for indicating the occurrence of groundwater contamination derived from the anthropic activities conducted in the PCM.

The different hydrogeochemical facies found in the aquifer system of the PCM comprises low mineralized Ca-$HCO_3$ water for the main Eocene karst aquifer, and Ca-$SO_4$ and highly mineralized Na–Cl water types in the minor aquifers discharging from the PCM. The NBL values of $SO_4$, Cl and $NO_3$ obtained for the main karst aquifer are 14.33, 4.06 and 6.55 mg/L, respectively. These values are 35, 3 and 1.2 times lower than the respective official NBLs values that were determined by the water administration to be compared with in the case of conducting a pollution assessment characterization in the main karst aquifer. Official overestimation of NBLs can put important groundwater resources in the PCM at risk.

**Keywords:** High-mountain karst system; Natural background levels; Compositional data; Model-based clustering; Gaussian mixing model.

# 1. Introduction

High mountain zones produce globally essential water resources that feed fresh water to the lowland depending ecosystems and a large portion of the world's population (Viviroli et al., 2020). Mountain aquifers, specially those developed in karstifiable carbonate rocks, store the infiltrated precipitation, thus maintaining important groundwater resources. These resources are typically released through large springs that regulates the hydro-ecological regime of the downstream rivers (Kresic and Stevanović, 2010), and provide water resources during the dry season in semi-arid regions, where they are often the primary source of drinking water (Stevanović, 2019).

Karst aquifers are much more vulnerable to pollution than other aquifers. Contaminants may easily enter the subsurface into the karst system and rapidly spread in the conduit system without any substantial attenuation (Marín and Andreo, 2015), threatening the water resources of a region, at large scale. These aquifers need special protection (Drew and Hötzl 1999, Zwahlen, 2004). In this line, the European Union enacted the Water Framework Directive (2000/60/EC) (WFD, 2000) as an integrated approach focusing on the monitoring of water bodies. The WFD (2000) also defines the rules for the identification of the different groundwater bodies (GWB), but also the criteria for chemical status assessment through defining pollutants threshold values (TVs) and

groundwater natural background values (NBLs). The TVs are quality standards for pollutants in groundwater representative of those groundwater bodies considered to be at risk. The NBLs provide the information regarding the concentration of a given element, species or chemical substance present in solution which is derived by natural processes from geological, chemical, biological and atmospheric sources (Müller et al., 2006). In other words, NBLs are the corner stone to quantitatively evaluate whether groundwater is significantly affected or modified by anthropogenic influences (Nieto et al., 2005; Custodio et al., 2007).

It is not easy to define NBLs in high mountain karst aquifer systems (HMKS). For a given aquifer and a certain component, the corresponding NBL value is obtained by averaging the dissolved content of that component in groundwater discharge for the different springs draining the aquifer. HMKS are usually embedded in geological structures that are the result of complex tectonic processes (e.g. faults, fold-and-thrust belts, wedge pinch out layers). This often causes a strong compartmentalization (Ballesteros et al, 2014) that may involve different lithologies (i.e. from carbonates to evaporites), thus generating a complex aquifer system. The geological variability of such aquifer system influences the hydrogeochemical signature of groundwater along the different flowlines, which typically converge while mixing around springs. As a result, a different hydrochemical composition than the expected may be obtained in the discharge of a spring given its geological setting (Lambán et al., 2015), thus complicating a consistent NBLs characterization for the different aquifers conforming the hydrogeological system.

To correctly define NBLs in HMKS it is fundamental to have both a good hydrogeological characterization and sound conceptual model of the aquifers at local scale, and a good characterization of the relevant hydrogeochemical fingerprints describing the whole picture of the aquifer system. In this framework, multivariate statistical analysis (MSA) techniques/tools have shown a proven track record in characterizing complex hydrogeological systems through the analysis of spatial variations in hydrochemical data.

Geochemical data (and hence also hydrogeochemical data) are compositional by nature. This means that the concentration of a given element is actually expressing a part of a whole, regardless of the dimensions in which the component concentration is expressed, either as weight per cent ratio (e.g., %, mg/kg), or given as component mass per unit of

dissolution volume (e.g., mg/L). Consequently, according to Aitchison (1986), they carry only relative information. In geochemistry and statistics they are known as 'closed data' which implies that they not vary independently. As a consequence, they are not well represented by the usual Euclidean mathematical real structure. This may lead to important drawbacks in the analysis, widely discussed by different authors (Reimann et al., 2012; Buccianti and Grunsky, 2014; Filzmoser et al., 2018; Pawlowsky-Glahn, et al. 2015), which can affect its direct use in MSA if the appropriate transformations are not previously done. To overcome the problem, Aitchison (1986) described mathematically the structure of the Simplex (the sample space for compositional data) and proposed the first log ratio approaches, such as the additive log ratio (alt) and centered log ratio (clr), in order to express the compositional data sets in the usual real space. Later on, Egozcue, et al. (2003) proposed the isometric log-ratio (ilr) coordinates, also known as 'balances'. The latter transformation has better mathematical properties, and most importantly, allows to better interpret intermediate results of the analysis. These sets of methods are usually refered as compositional data (CoDa) analysis and allow to 'open' geochemical data, transforming the raw data before the application of classical MSA tools. The CoDa approach has been widely used in soil geochemistry studies (Buccianti et al., 2018; Carranza, 2011; Reimann et al., 2012, among others) and less often for hydrogeological studies, (Blake et al., 2016; Bondu et al., 2020; Otero et al., 2005; Owen et al., 2016, among others). In some cases this has already been used specifically for NBL studies.

The combination of MSA tools (e.g. principal component analysis and clustering analysis) allow to investigate the factors controlling the processes taking place in aquifers driving the hydrogeochemical composition of groundwater (Puig et al., 2011; Blake et al., Piña et al., 2018; Shelton et al., 2018). Clustering analysis (CA) methods have been largely used to separate groundwater samples, especially for large and/or complicated datasets, into homogeneous groups to show up different source contributions to groundwater in the sampled springs (see Suk and Lee, 1999; Cloutier et al., 2008; Yidana, 2010; Kim et al., 2014; Yolcubal et al., 2019, among others). This faculty makes CA methods a promising tool to correctly define NBLs in HMKS.

There are two mainstreams in CA, (1) the "hard clustering" methods like hierarchical clustering and partitioning methods (k-means, k-medoids: Partitioning Around Medoids – PAM -, and Clustering Large Applications – CLARA), where each data point (i.e. the

sample) is assigned to one and only one cluster (hard assignment), and (2) the "soft clustering" methods, like model-based clustering (e.g. the Gaussian Mixture Models – GMM) and fuzzy clustering where instead of assigning each data point into a unique specific cluster, it is assigned to all the clusters with different probabilities or weights (soft assignment) (Güler and Thyne, 2004).

Soft clustering methods are getting more popular since they provide degrees of membership at different hydrogeochemical clusters, rather than clear-cut distinctions. As a result, they can better reflect the spatial continuity of a hydrological system while providing a more rigorous framework to validate the clustering results (Kim et al., 2014; 2015; Wu et al., 2017; Bondu et al., 2020). Moreover, in the framework of HMKA where the limited number of observations often is a challenge, GMM clustering algorithms are shown to be able to provide valuable insights into hydrochemical processes, delineating the different groundwater sources imprinting the hydrochemical signature of the aquifer system, despite a sparse hydrochemical dataset (Wu et al., 2017). GMM are specially well suited to provide a solid basement for NBLs determination in HMKS. Altough GMM have been used for some authors to evaluate NBLs (Kim, et al. 2015), surprisingly, there are no references in the scientific literature using GMM in the framework of CoDa analysis to evaluate NBLs in HMKS.

This work aims at filling this gap. To that end, we characterize the hydrochemical composition of the different aquifers associated to the alpine karst aquifer system of the Port del Comte Massif (PCM) to evaluate in a consistent way the NBLs for the different aquifers integrated in this HMKS. This is conducted through a MSA approach that combines in a CoDa analysis framework both PCA and GMM clustering analysis.

## 2. The study area

The PCM is located in the South-Central Catalan Pyrenees (north-east of Spain), which constitute an orogenic system that runs along the boundary between the Iberian and European plates. It is of Late Cretaceous to Miocene age (Muñoz, et al 2018). The elevation of the mountainous massif ranges from 900 m a.s.l. to 2390 m a.s.l. The massif constitutes an independent structural and hydrogeological system with a surface area of

167 110 km$^2$. The highest peaks of the massif conform a water divide between the upper Segre
168 River basin to the NW and SW (a large tributary in the Ebro basin) and the upper Cardener
169 River basin (a tributary of the LLobregat River) to the SE (Fig. 1).
170
171 According to the Köppen-Geiger classification (Peel et al., 2007), the study area is
172 characterized by a cold climate without a dry season and with a temperate summer. For
173 the period 2005-2019, the average annual precipitation (P), temperature (T) and potential
174 evapotranspiration (Hargreaves' method) at the SMC meteorological station located at
175 2315m a.s.l. (Fig. 1) are 1055 mm, 3.2° C and 525 mm, respectively. At elevations > 1800
176 m a.s.l. the snow covers the massif from December to March.
177

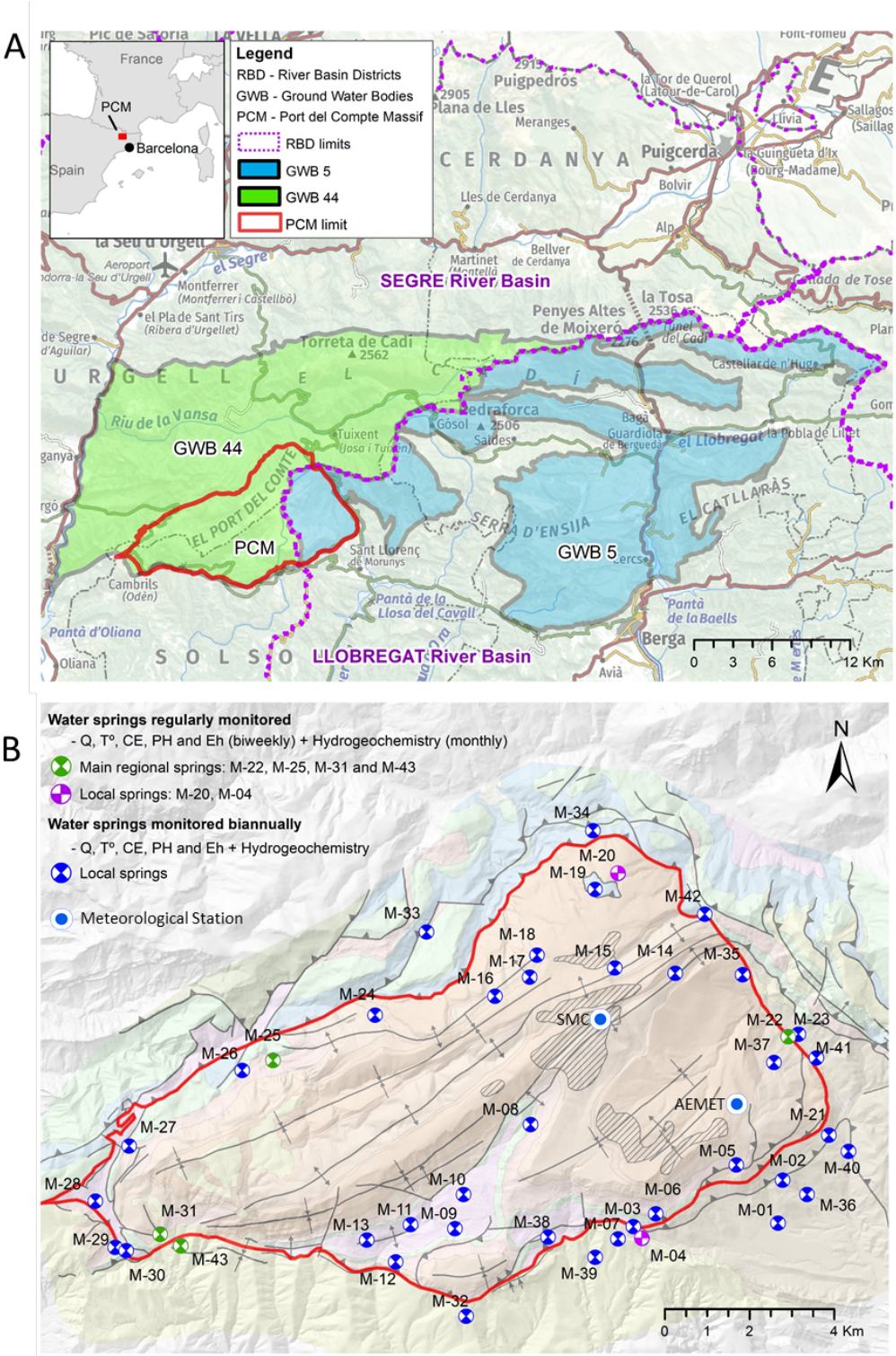


**Fig.1.** (A) Location map of the study area. (A). Delimitation of the groundwater bodies affecting the PCM; GWB-44 belongs to the Segre river basin, and GWB-5 belongs to the Llobregat river basin. (B) Location of the 43 monitored springs in the PCM

184 Geologically, the PCM constitutes an independent thrust sheet which presents complex
185 structural shapes in its boundaries (Fig. 2), with different thrust sheets individualizing the
186 whole domain in one independent structural system. The internal structure of the PCM is
187 formed by a set of folds and thrusts. These folds have a constant direction NE-SW parallel
188 to the NW limit (Vergés, 1999). The stratigraphic series contains limestones and
189 evaporites mainly from the Triassic, Cretaceous limestones, Paleogene calcarenites, and
190 shales, and Eocene-Oligocene limestones, sandstones and marls. The Jurassic marls,
191 limestones and dolomites only outcrops in the NW part of the geological sheet. The
192 limestones have a total thickness greater than 1300 m. From the geomorphological
193 perspective, the PCM presents a rounded-soft landscape in the highest domains with no
194 vegetation cover and almost no soil horizon development. The rest of the massif is
195 covered by mountain meadows and forest, with a shallow soil depth up to medium
196 development ground cover. Many different karst forms appear progressively from 1950
197 m.a.s.l. upwards, being well developed at 2050m a.s.l. (see Fig 2, indicated as 'Area with
198 well-developed karst landforms'), with sinkholes, dolines and karren fields. They
199 underline the heterogeneity of the karst system.
200
201 From the hydrogeological point of view, the PCM can be considered an independent unit
202 multi-aquifer system. The main aquifer is formed by Lower Eocene – fissured and
203 karstified limestones and dolomites. It constitutes one of the most important karst aquifers
204 of the Catalan Pyrenees. The other existing aquifers and aquitards in the system are related
205 to the Cretaceous limestones, Triassic limestone and evaporites, other Paleogene
206 conglomerates and sandstones, and also to small Quaternary aquifers draining small
207 areas, which can be recharged locally at low or medium elevations. The lower Upper
208 Cretaceous/Paleocene (Garumnian facies) substrate materials, composed by siltstone and
209 shales constitute an impervious layer for the overlaying Lower Eocene karst aquifer. The
210 geometric characteristics of the geologic structure of the system strongly influences the
211 location of the existing karst springs, their groundwater geochemistry and their long-term
212 hydrologic behaviour.
213

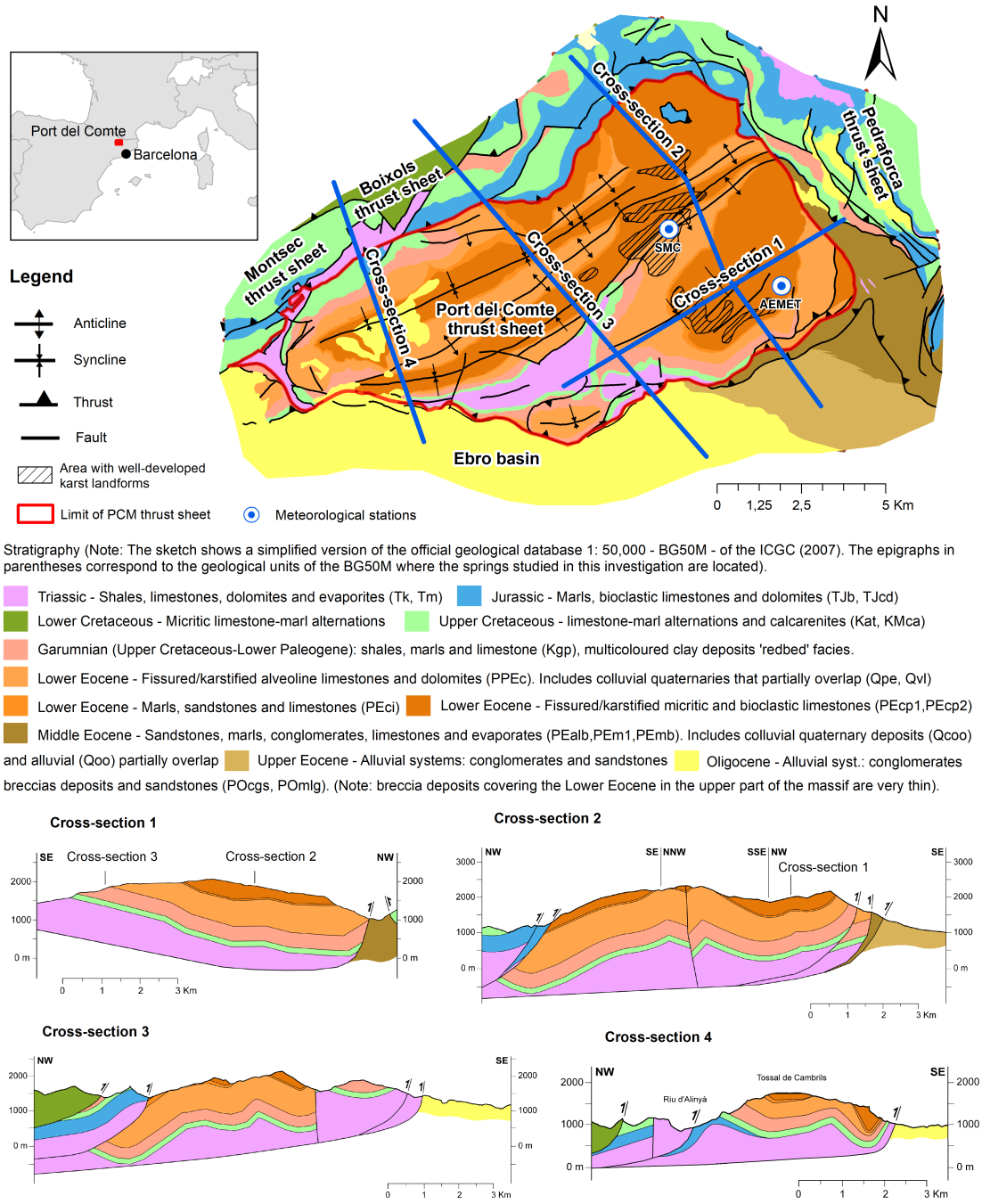


214

215 **Fig. 2.** Geological map and geological cross-sections of the PCM (modified from ICGC,
216 2007)

217 The hydrogeological conceptual model of the PCM aquifer system, as presented by
218 Herms, et al. (2019), considers that recharge is produced by infiltration of precipitation
219 as rainfall and snowmelt, and occurs both concentrated through the local karst conductive
220 features, mostly situated at the top of the massif, and diffuse through the whole domain.

The infiltrated water percolates through the thick unsaturated zone (more than 1000 m at the top of the massif) towards the saturated zone, and discharges through a large number of springs.

More that 100 springs were inventoried in the study zone. Nevertheless, only 43 of them discharge throughout the year (Fig. 1). These springs were monitored during the period September 2013 – October 2015. Most of them discharge small-scale local sub-surface water flows, with flow rates ranging between 0.1 L/s to 1 L/s. Nevertheless, there are four 'regional' springs (M-22, M-25, M-31 and M-43) with flow rates between 1 L/s and 900 L/s during the monitored period. These regional springs are recharged at medium to high elevations, and drain the system discharging through the limestones outcrops (M-31), Quaternary deposits overlying the limestones (M-25, M-22), and also through well-developed karst conduits in the conglomeratic materials of the Ebro Basin (M-43). These conglomerates conform the southern foreland basin of the Pyrenees, which is located just at the southern border of the PCM. There is also a diffuse groundwater discharge through the 'Riu Fred' sub-basin, to the North. With the exception of two singular groundwater wells on the SW and E edges of the PCM, there are no other water wells within the perimeter of the PCM that exploit the main karst aquifer. It is estimated that the regional water table of the karst system is between 1000 and 1100 m a.s.l. (Herms et al., 2019).

Although the whole PCM massif belongs to the same geomorphological structure, the SE sector has been assigned to GWB-5 ('Conca Alta del Cardener i Llobregat'), whereas the rest of the PCM was assigned to GWB-44 ('Cadí Port del Comte'). Table 1 summarizes the natural background levels at the 90$^{th}$ percentile values (NBL90), determined through the Pre-selection (PS) method described by the EU research project "BRIDGE" (2007) (Müller et al., 2006) using different control points for each GWB. It is worth noting the high values for $SO_4$ contents in both GWBs. The NBLs values are assigned to the entire GWBs, and therefore are understood as representative of all units / aquifers included in these bodies. However when the focus is on particular aquifers such as the pristine waters related to the Eocene karst aquifer included in the PCM, the assigned input value appears high.

**Table 1.** NBL90 values for Cl, $NO_3$ and $SO_4$ in the GWB-5 and GWB-44.

| | NBL90 | | |
|---|---|---|---|
| | Cl [mg/L] | $SO_4$ [mg/L] | $NO_3$ [mg/L] |
| GWB-5 | 12 [a] | 485 [a] | - |
| GWB-44 | 36[b] | 609[b] | 8[b] |

(a) Data source: Agència Catalana de l'Aigua

(b) Data source: Confederación Hidrográfica del Ebro

In the current Spanish regulation for drinking water (MHCASWS, 2003) the limit of potability for sulfate is 250 mg/L of $SO_4$. According to this value, the whole GWB5 and 44 would be exceeding the regulatory limit, when groundwater from the Eocene aquifer is actually being used safely for drinking downstream. Therefore, assigning a global NBL value when the GWB integrates a number of aquifers with a different hydrochemical signature is not a minor issue.

# 3. Materials and methods

## 3.1. Sampling and analysis

In this work, 43 springs were sampled twice per year (i.e. before snowfall and after snowmelt seasons) between September 2013 and October 2015. Nevertheless, in six of them (M-04, M-20, M-22, M-25, M-31 and M-43) (Fig. 1) the groundwater sampling frequency was higher, every three to four weeks, to study the hydrogeochemical evolution of groundwater discharge. The springs M-22, M-25, M-31 and M-43 correspond to regional discharge points of the karst system, whereas springs M-04 and M-20 are considered representative of the local small aquifers of the area (Herms et al., 2019).

A total of 288 groundwater samples were collected. Additionally, 10 snow samples (7 from natural snow and 3 from artificial snow produced in the existing ski resort in the NE zone of the PCM) and two water samples from water ponds used to artificial snow production were collected. In all cases, the in situ physico-chemical parameters Temperature (T), electrical conductivity (EC), pH, Eh and the total dissolved solid (TDS) were measured. The geochemical analysis considered major cations and anions.

All samples were filtered using a 0.45µm membrane filter and stored in new 200-500 mL polyethylene bottles washed with diluted nitric acid and rinsed with the water to be sampled prior to sampling. Samples for cation analysis were acidified with ultrapure

283 $HNO_3$, to pH<2 to prevent precipitation. Samples for anion analysis were not acidified.
284 All water samples were preserved at 4 ºC before laboratory measurement. T, CE, pH, Eh
285 and TDS were measured by a portable Hanna meter (Multiparameter Water Quality Meter
286 HI9829). The total alkalinity was determined in situ using the titration method - and later
287 for the rest of campaigns using a photometer colorimetric method with the HI755
288 alkalinity test checker (Hanna Instruments). The major cations (Ca, Mg, Na, K, $NH_4$) and
289 anions (Cl, $NO_3$, $HCO_3$,$CO_3$, $SO_4$, and F) were determined in the Laboratori Ambiental
290 d'Aigües de Terrassa: the cations were analysed by inductively coupled plasma atomic
291 emission spectrometry (ICP-OES Agilent 5100 DV), except the ammonium, which was
292 measured using a ultraviolet-visible (UV-VIS) spectrophotometer, and the anions by ion
293 chromatography (Dionex, DX-120). Ionic balance errors were calculated using the USGS
294 software PHREEQC (Parkhurst and Appelo, 2013) within the version PhreeqC
295 Interactive (version 3.3.3 10424), and with the phreeqc.dat database, except for the most
296 salinized natural waters (M-30 and M-41) related to deep flow through Keuper
297 evaporates. The majority of analyses had ionic balance errors below the recommended
298 standard of ±5% (Appelo and Postma, 2005).
299

300 **3.2 Data transformation using the CoDa approach**

301 Geochemical datasets contain mostly compositional variables. , that is, multivariate
302 variables where the individual parts are parts of a whole (Buccianti and Grunsky, 2014).
303 Classical examples refer to constant sum variables, but recent definitions of
304 compositional data include all types of data representing parts of some whole. Ignoring
305 the compositional character of these geochemical variables may lead to misleading results
306 (Pawlowsky-Glahn et al., 2015). In this context, the CoDa analysis methodology is used
307 in this work. In order to avoid the problems derived from the compositional data
308 character, three transformations, all based on log-ratios have been historically proposed,
309 named as: additive log-ratio (alr) transformation, centered log-ratio (clr) transformation
310 (Aitchison, 1986) and isometric log-ratio (ilr) transformation (Egozcue et al., 2003).
311

312 In this study, the hydrochemical dataset was transformed using, firstly clr and secondly
313 ilr. If $\mathbf{x}$ is the compositional vector, $\mathbf{x} = (x_1, \ldots, x_n)$, the former transformation is
314 described by
315

$$\mathrm{clr}(\mathbf{x}) = ln\left(\frac{x_i}{g(x_i)}\right);\ i = 1 \div D, \quad (1)$$

where $g(\mathbf{x}) = \sqrt[D]{\prod_{i=1}^{D} x_i}$ is the geometric mean of all the considered components (ions), and $D$ is the column matrix dimension.

The ilr transformation allows to express hydrochemical compositions with respect to an orthonormal basis. Their coordinates, called balances, may be easily obtained using a Sequential binary partition (SBP) (Egozcue et al., 2003; Egozcue and Pawlowsky-Glahn, 2005, 2006; Pawlowsky-Glahn et al. 2015). The SBP has been widely used for many authors on water chemistry studies (Engle and Rowan, 2013; Owen et al., 2016; Hee Kim et al., 2019; Bondu et al., 2020). For a D column matrix, i.e. a D-part composition, D-1 balances are calculated from the SBP as

$$\mathrm{ilr}(\mathbf{x}) = \sqrt{\frac{r_{i_+} \cdot r_{i_-}}{r_{i_+} + r_{i_-}}} \ln \frac{g(c_{i_+})}{g(c_{i_-})};\ \ i = 1 \div D - 1\,, \quad (2)$$

where $c_{i_+}$ and $c_{i_-}$ are the groups of parts separated in the $i^{\text{th}}$ step of the SBP; $r_{i_+}$ and $r_{i_-}$ are the numbers of parts included in $c_{i_+}$ and $c_{i_-}$, respectively.

According to Egozcue and Pawlowsky-Glahn (2005; 2006), two methods for performing SBP can be applied: (1) directly from the PCA, and (2) by experienced judgment, where non-overlapping groups of parts, known as balances, are defined.

There are different software tools that allow to perform these transformations. The called CoDaPack v.2.0. program (Comas-Cufi and Thió-Henestrosa, 2011) is a software developed by the Research Group in Statistics and Compositional Data Analysis at University of Girona (UdG). This software can be freely downloaded from http://ima.udg.edu/codapack. It allows performing the log-ratio transformations and to prepare different kind of plots to show the results. In this research, all statistical analyses were done using the statistics program R version 3.6.1 (2019-07-05) (R Development Core Team 2004), which is available for free under the GNU-public License and for all platforms from http://www.cran.r-project.org, through the software RStudio, a graphical user interface for R . For multivariate statistical analysis (MSA) using the CoDa analysis approach, the following packages for R software were used: {stats} version 3.6.1. (R-core

R-core@R-project.org); {compositions} version 1.40-5 (Van den Boogaart and Tolosana-Delgado, 2008) {zCompositions} version 1.3.4 (Palarea-Albaladejo and Martín-Fernández, 2015).

Water samples with solute dissolved concentrations lower than the detection limit (the so-called 'left-censored values') put an extra challenge when addressing MSA techniques. The censored data can be either removed, or replaced or imputed (e.g. values below detection limit are rounded as zeros) (Carranza, 2011). Following the criteria used for several authors (Reimann and Filzmoser, 2000; Farnham et al., 2002), in this work, left-censored values were excluded from the MSA when they represented > 25% of the total number of samples (i.e. when the variable had a 'medium–high' level of nondetects according to Palarea-Albaladejo and Martín-Fernández, 2014). Different algorithms can be applied within the {zCompositions} package for R for imputing these values (like multRepl, multLN, lrEM and lrDA methods).

### 3.3. Univariate exploratory data analysis

In order to explore the internal structure of the datasets, different Exploratory Data Analysis (EDA) plots combining an histogram, density trace, one-dimensional scatterplot and a boxplot (Kürzl, H. 1988) were used. Having this in mind, the ilr coordinates are adapted to the univariate case with the package {StatDa} (Filzmoser et al, 2009, 2009b). The variable of interest $x$ (i.e. Cl, $NO_3$ and $SO_4$) is single ilr-transformed (Eq. 3):

$$z = \frac{1}{\sqrt{2}} \cdot ln\left(\frac{x}{1-x}\right) \quad (3)$$

### 3.4 Principal Component Analysis (PCA) and Model-based clustering

The first step to apply any MSA, is to check the presence of left-censored data and the imputation of values. The function 'zPatterns' {zCompostions} is used to find and display patterns of zeros/missing values in the whole dataset (see pattern diagrams at Fig.SM.2.1 of Supp. Mat.). In this work, the left-censored detected values were imputed using the 'lrDA' (log ratio Data Argumentation) function. It is based on the log ratio Markov Chain Monte Carlo Data Argumentation algorithm (Palarea-Albaladejo and Martín-Fernández,

2015), and it has been already used by different authors to delineate water types (e.g. Owen et al 2016; Hee Kim et al., 2019). Following the commented procedure two data matrices were prepared:

- Dataset Matrix (300x8), corresponding to 300 water samples (288 groundwater samples and 12 snow and water ponds samples) and 8 variables ($HCO_3$, Cl, $SO_4$, $NO_3$, Ca, Mg, Na, K).

- Dataset Matrix (43x8), corresponding to the median hydrochemical composition of groundwater evaluated for each of the 43 springs and 8 variables ($HCO_3$, Cl, $SO_4$, $NO_3$, Ca, Mg, Na, K) (Table SM.1. Supp. Mat.) The consideration of "median composition" of time series follows the requirements to estimate NBL's using the PS method (see section 3.4).

Table SM.3.1 (Supp. Mat.) shows the list of parameters 'included' and 'excluded' for the MSA and their justification.

PCA is a very common method that is based on dimensionality reduction of datasets. It helps deciphering hydrogeochemical patterns and to infer the controlling variables of the water chemistry (Merchán et al., 2015; Moya et al., 2015). In order to perform the PCA it is necessary to calculate the '*variation matrix*' of the dataset (Aitchison, 1986) as a first step to obtain a measure of the dependence of the different variables, that is, the parts of the composition. Each component of the variation matrix, $\tau_{ij}$, describes the log-relationship between two of the composition $x_i$ and $x_j$ (in this case chemical species). It is defined as

$$\tau_{ij} = \mathrm{var}\left(\ln\frac{x_i}{x_j}\right) = \frac{1}{N-1}\sum_{n=1}^{N}\ln^2\left(\frac{x_{ni}}{x_{nj}}\right) - \ln^2\left(\frac{g_i}{g_j}\right), \quad (4)$$

where N is the number of observations and $g_i$, $g_j$ are the geometric mean values for the two variables considered. A small value of $\tau_{ij}$ (which is equivalent to $\tau_{ji}$) implies a good proportionality between the two variables. The variation matrix, $\tau_{ij}$, is obtained using the R function 'summary.acomp' of the package {compositions}.

Once the variation matrix is obtained, then the correlation between the variables $x_i$ and $x_j$ is estimated through the '*index of proportionality*' function, $\rho_{ij}$ (Eq. 5) (Aitchison, 1986). The stronger the correlation between $x_i$ and $x_j$ the closer to 1 is the value of $\rho_{ij}$.

$$\rho_{ij} = \exp\left(\frac{-\tau_{ij}^2}{2}\right) \quad (5)$$

Data transformation following the CoDa analysis approach is applied before using any MSA tool. In this case, the PCA is applied using clr-transformed data (Eq. 1) obtained with the function 'clr' of the {compositions} R package. The method provides a new matrix of standardized coordinates for each sample called 'the scores', and also a new matrix of variable 'loadings' with columns representing the principal components of the (clr-transformed) data.

The graphical representations of the PCA results of clr-transformed data were done using the well-known biplot graphic (Gabriel, 1971) (Fig. 3), where the individuals are expressed as dots and the variables as rays. However, the interpretation of the clr-biplot differs from the interpretation of the classical biplot. Te clr-biplot interpretation is conducted by following the criteria proposed by Aitchison and Greenacre (2002), which is well suited for analyzing compositional data (Otero et al., 2005; Engle and Rowan, 2013; Blake et al., 2016; Piña et al., 2018). The criteria can be summarized as:

- The length of a link (i.e . black shaded line) between the rays (red arrows) defining clr($x_i$) and clr($x_j$) is proportional to the variance of ln($x_i$/$x_j$).
- If two rays lay near each other, their quotient might be almost constant, and they might be proportional.
- If two links between four different clr-variables are orthogonal, then the corresponding pairwise quotients may be independent.
- If three or more vectors lie on the same link, the corresponding sub-composition might have one single degree of freedom.
- If two links between four separate clr-variables are orthogonal then the corresponding pairs of variables may vary independently of each other.

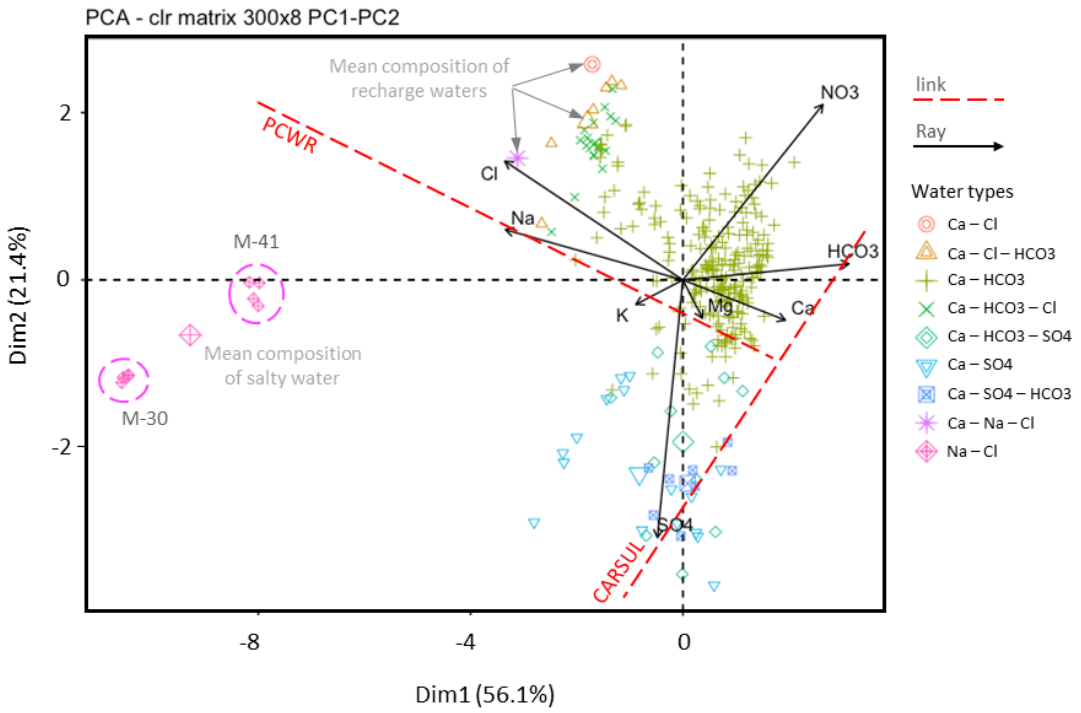


439
440

441 **Fig. 3.** clr-Biplot of the Principal Components PC1 and PC2 for the dataset Matrix
442 (300x8). The label of the axes indicates the percentage of the variance explained by PC1
443 and PC2, respectively. The PCWR dashed line indicates the link between pristine waters
444 and groundwater with water-rock interaction. The CARSUL dashed line indicates the link
445 between CARbonate and SULphate waters. The smaller circles correspond to the
446 different water samples and their color indicates their corresponding water type, whereas
447 the larger circles represent the average composition of the different water types. To
448 illustrate this, the groundwater samples from springs M-30 and a M-41 are indicated, as
449 well as the corresponding mean composition.
450
451 The principal aim of cluster analysis is to split a number of observations into groups that
452 are similar in their characteristics or behaviour (Reimann et al. 2008). The cluster analysis
453 is applied to group observations into several homogeneous clusters. It is based upon
454 similarities between the observations and provides insights regarding the multivariate
455 geochemistry characteristics (Bondu et al., 2020; Templ et al., 2008).
456
457 In this work it is used the 'soft' model-based clustering method. One of the main
458 advantages is that it uses a probability-based approach. Therefore, the obtained partition
459 can be interpreted from a statistical point of view, unlike the classical 'hard' - or heuristic-

based - algorithms (k-means, hierarchical clustering, etc.) (Bouveyron and Brunet-Saumard, 2014). The model-based clustering approach used considering the ilr-transformed data was the finite mixtures of multivariate-normal or Gaussian distributions known as Gaussian Mixture Model (GMM), which is included in the {Mclust} R package (Fraley and Raftery, 2002; Fraley et al. 2012; Scrucca et al., 2016), and using the R version: 5.4.6 (Raferty et al., 2020). It assumes that observed data come from a mixture of underlying probability distributions representative of two or more clusters.

The GMM assumes the following probability distribution function (PDF)

$$f(x) = \sum_{k=1}^{K} \omega_k f_k(x|\mu_k, D_k) \ , \tag{6}$$

where $\omega_k$ represents the weight or mixing proportion ($0 \leq \omega_k \leq 1$; $\sum_{k=1}^{K} \omega_k = 1$) or probability that an observation comes from the $k_{th}$ mixture component, K is total number of components (i.e., groups or clusters), and $f_k$ is the PDF of the observations for the $k^{th}$ variable. Each component is usually modeled by a normal distribution (Eq. 7) with mean $\mu_k$ and covariance matrix $D_k$.

$$f_k(x|\mu_k, D_k) = \frac{1}{(2\pi)^{\frac{p}{2}} \cdot |D_k|^{\frac{1}{2}}} \exp\left[-\frac{(x-\mu_k)^2}{2 \cdot D_k}\right] \tag{7}$$

Taking into account Eq. 6 the conditional probability of assigning one observation to a given cluster is given by

$$P(cluster\ k|x) = \frac{\omega_k f_k(x|\mu_k, D_k)}{f(x)} \tag{8}$$

The greater the value of P the closer the association of sample x with the PDF corresponding to the cluster k is. By definition, those samples for which P > 0.5 for PDF $k$ constitute a ‘‘cluster’’.

For the different components $K$, the model parameters $\omega_k$, $\mu_k$, and $D_k$ are estimated using the expectation–maximization (EM) algorithm (Dempster et al., 1977). The covariance matrix $D_k$ describes the geometry of the clusters with its volume, shape and orientation The different combinantions of these parameters allows to define 14 multivariate mixture

models grouped in three main families: spherical, diagonal and ellipsoidal, which are included in the version used of {Mclust} package. In the other hand, this package uses the Bayesian Information Criterion (BIC) to find the optimum number of clusters. It identifies from those 14 multivariate mixing models, the one that best characterizes the data while maximizing BIC. More details of the GMM, BIC and EM mathematical approach, can be found on Biernacki and Govaert (1999), Fraley and Raftery (2002, 2012) and Raferty et al. (2020). In this study, model-based clustering has been applied to the dataset Matrix (43x8) of major ion data ($HCO_3$, Cl, $SO_4$, $NO_3$, Ca, Mg, Na, K), represented in this case using ilr-coordinates (Eq. 2).

The use of "hard" clustering methods were also analysed using the {clValid} (Brock et al. 2008), the {factoextra}R package (Kassambara and Mundt, 2016) and the {NbClust} R package (Charrad et al. 2014). Considering the results obtained, it was decided to rule out their use in front of the GMM in order to avoid the degree of subjectivity in the choice of the most suitable options for determining the relevant number of clusters and the best 'hard' method with the 43x8 matrix dataset. The results obtained can be consulted in the Supplementary Material.

### 3.5. Determination of Natural Background Levels (NBLs) and Threshold Values (TV)

After identifying the number of underlying clusters in the data set in hand, based on MSA tools, the NBL and TV values for Cl, $SO_4$ and $NO_3$ are determined, which are the most common solutes causing specific groundwater pollution issues in HMKS. In this work, the PS-method developed in the framework of the EU "BRIDGE" (2007) project (Müller et al., 2006) is applied since it has been successfully proven in many studies (Coetsiers et al., 2009; Ducci and Sellerino, 2012; Hinsby et al., 2008; Marandi and Karro, 2008; Parrone et al., 2019; Preziosi et al., 2010; Wendland et al., 2008; Zabala et al., 2016). The PS-method considers the following criteria for data preparation before estimating the NBL's:

- Time series should be replaced by medians (i.e. all sampling sites contribute equally to the NBL estimation).

- Samples with incorrect ion balance (exceeding 10%) and samples with median $NO_3$ contents >10 mg/L must be rejected.
- Brackish waters (i.e. NaCl) exceeding 1 g/L must not be considered.
- If samples are anaerobic ($O_2$ < 1 mg/L) or denitrification occurs, the dataset needs to be evaluated for the aerobic and anaerobic samples separately.

To obtain the NBL, the 90$^{th}$ percentile of the data sets is advisable for small datasets (N ≤ 60 sampling points) or when human impact cannot be excluded from the data, which is the case of the case study in this research. For n > 60 the 97.7$^{th}$ percentile is preferred. Once the NBLs are defined then the TVs are obtained following the final methodology suggested by the EU "BRIDGE" project:

$$TV = \begin{cases} \frac{1}{2} \cdot (\mathrm{NBL} + \mathrm{Ref}); & NBL \leq Ref \\ NBL; & NBL > Ref \end{cases}, \quad (9)$$

where *Ref* is the reference value. In case of the Spanish Royal Decree 140/2003 of 7 February, laying down the health criteria for the quality of water intended for human consumption, the values of *Ref* for $SO_4$, $NO_3$ and Cl are 250 mg/L, 50 mg/L and 200 mg/L, respectively.

# 4. Results and discussion

## 4.1. Exploratory analysis of data and general water chemistry

The resulting EDA plots histograms for Cl, $NO_3$ and $SO_4$ of the dataset Matrix (43x8) (Fig.4.) show multi-model shapes in all the cases (i.e. major ions) suggesting that different populations are superimposed. In order to explain the dataset, and considering the geological setting of the area, a hypothetical mixture model with multiple components of different natural geogenic origin (possibly affected with local anthropogenic sources) must be considered, further to that coming from atmospheric deposition and evapo-concentrated in the soil and top rock. Thus, a simply bi-modal distribution composed of natural vs anthropogenic contamination cannot be considered to establish the NBLs

without taking into account the multivariate character of the data. Thus, the first step is to separate the chemical groups or clusters.

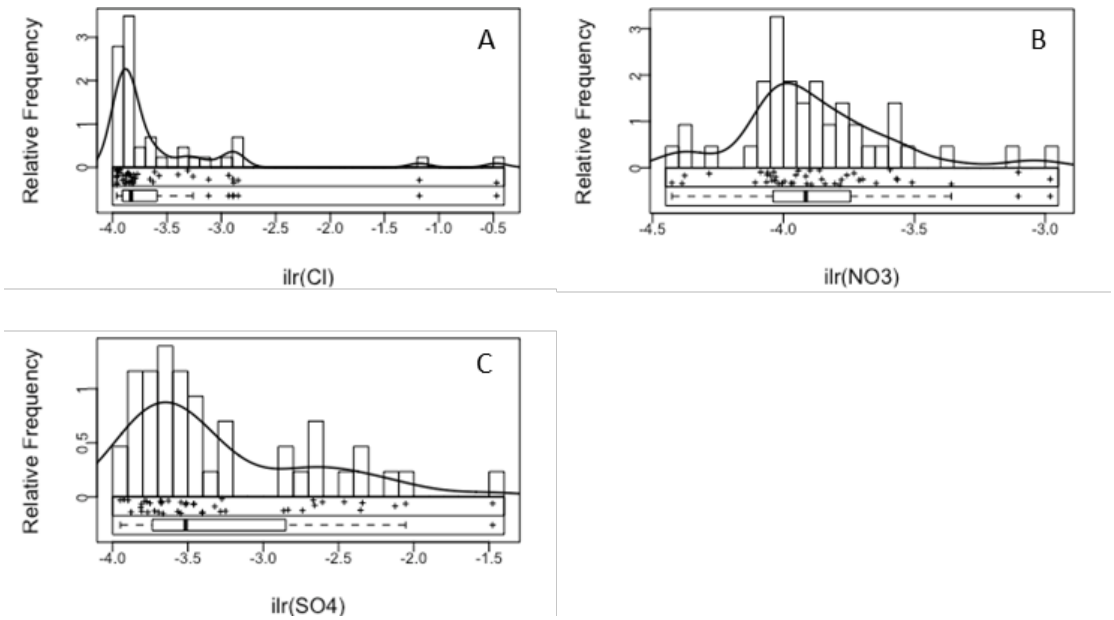


**Fig. 4** EDA plots of ilr transformed data for Cl (A), $NO_3$ (B), and $SO_4$ (C) of the Matrix (43x8).

Classical graphical methods for the classification of water chemistry data, such as Piper and modified Stiff diagrams were used as a first step to analyse the whole dataset (except water samples from pluviometers (i.e. in total 288 samples). Fig. 5 shows a map with the modified Stiff diagrams distribution over the PCM and also the corresponding modified Piper diagram. Based on that information, it is possible to initially aggregate the groundwater discharge from the 43 springs into 6 types of hydrogeochemical facies (Table 2):

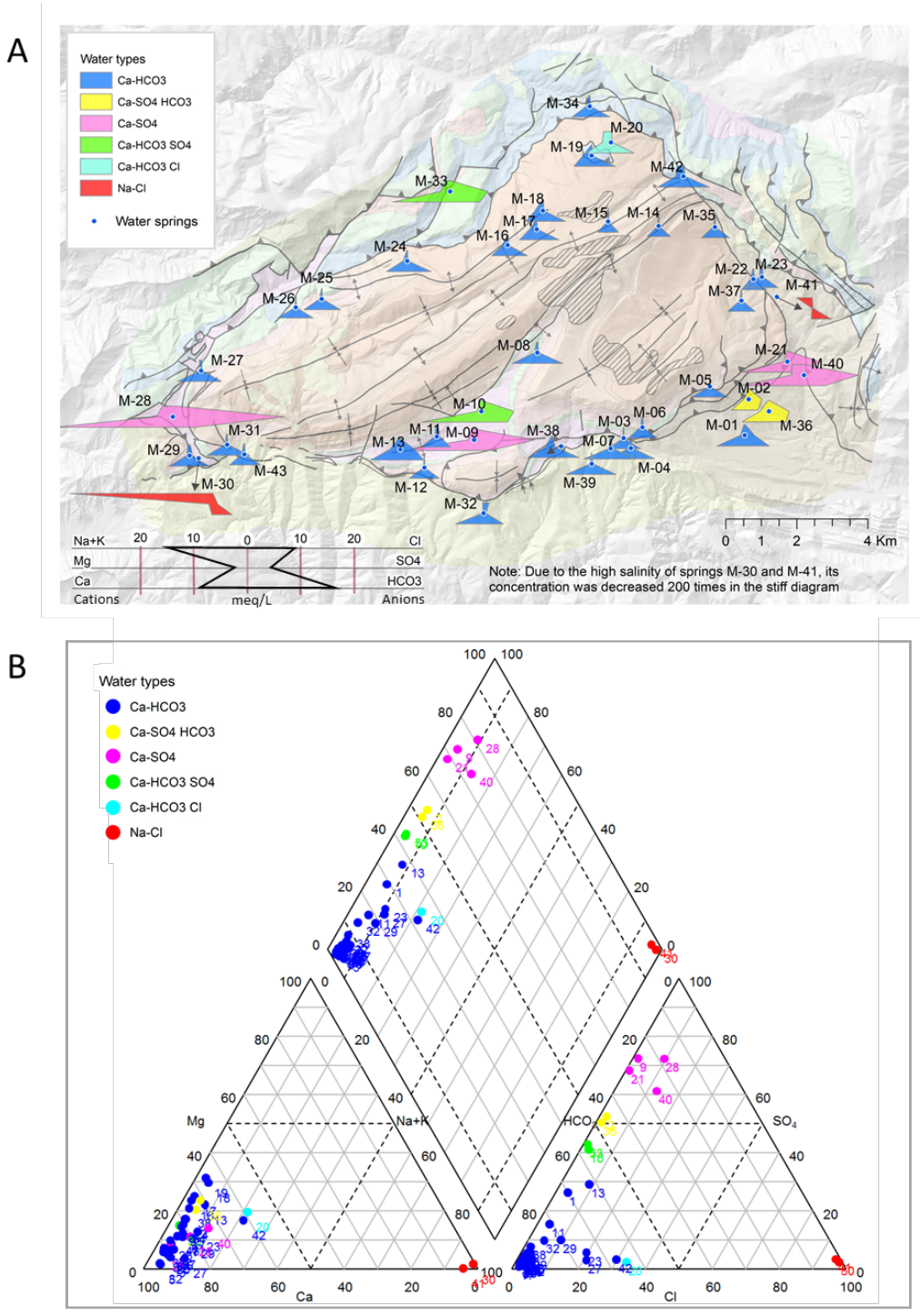


565

566 **Fig. 5.** Hydrochemical diagrams. (A) Modified Stiff diagram map and (B) Piper diagram
567 associated to the selected springs in the PCM. In both cases, for every spring the ion
568 content values correspond to the median value associated to all samples taken from that
569 spring. The springs are classified by their hydrochemical facies.

570

571 **Table 2.** Identified water types

| Water type | Num. Springs | Geological units[a] |
|---|---|---|
| $Ca\text{-}HCO_3$ | 32 | Cretaceous (KMca, Kgp, Kat)<br>Paleogene-Eocene (PEab, PEci, PEcp1, PEm1)<br>Paleogene-Oligocene (POcgs, POmlg, PPEc)<br>Quaternary (Qpe, Qt0, Qvl)<br>Triassic-Jurassic (TJb, TJcd)<br>Triassic Muschelkalk (Tm) |
| $Ca\text{-}HCO_3\text{-}Cl$ | 1 | Paleogene-Eocene (PEcp2) |
| $Ca\text{-}SO_4$_ | 4 | Quaternary (Qcoo)<br>Triassic-Keuper (Tk) |
| $Ca\text{-}HCO_3\text{-}SO_4$ | 2 | Triassic-Keuper (Tk) |
| Na-Cl | 2 | Triassic-Keuper (Tk) |
| $Ca\text{-}SO_4\text{-}HCO_3$ | 2 | Paleogene-Eocene (Pemb) |

(a) For a given Water type, the geological units based on ICGC, (2007) ordered by number of springs

572

573 At the first glance, the results show that diverse springs outcropping from different
574 geological units (ICGC, 2007) show similar groundwater facies, or also the same facies
575 can be obtained from different points located at different geological units. In this context,
576 these graphical techniques should not be considered determinant alone to discriminate
577 between hydrochemical groups and therefore, their results should be considered
578 preliminary. Table SM.1.1 (Supp. Mat.) shows the summary of the major ions content of
579 the 43 monitored springs (expressed as median values of time series for the period
580 September 2013 – October 2015) and also the water facies associated to them.

581

582 **4.2. PCA and dataset matrix size**

583 The variation matrix for the dataset Matrix (300x8) (Table 3) shows strong correlations
584 between different pairs of variables such as Ca and $HCO_3$, Na and Cl, and Mg and $HCO_3$.
585 Besides, $NO_3$ shows a high correlation with Ca and $HCO_3$, whereas almost no correlation
586 with $SO_4$. This result indicates that the most groundwater samples affected by nitrate
587 pollution are those from the Eocene karst aquifer with a $Ca–HCO_3$ hydrochemical
588 composition.
589

**Table 3.** The upper triangle over the main diagonal shows the '*index of proportionality*' (Eq. 5) of the dataset Matrix (300x8). The lower triangle over the main diagonal shows in italic the *'index of proportionality'* of the dataset Matrix (43x8). In both cases, the correlation values larger than 0.5 are shaded in blue.

| | Ca | Mg | Na | K | $HCO_3$ | Cl | $NO_3$ | $SO_4$ |
|---|---|---|---|---|---|---|---|---|
| Ca | -- | 0.88 | 0.06 | 0.51 | 0.98 | 0.04 | 0.57 | 0.44 |
| Mg | *0.76* | -- | 0.34 | 0.69 | 0.67 | 0.26 | 0.27 | 0.52 |
| Na | *0.01* | *0.10* | -- | 0.54 | 0 | 0.96 | 0 | 0.15 |
| K | *0.49* | *0.75* | *0.58* | -- | 0.15 | 0.36 | 0.13 | 0.43 |
| $HCO_3$ | *0.94* | *0.41* | *0* | *0.07* | -- | 0 | 0.56 | 0.06 |
| Cl | *0.01* | *0.07* | *0.99* | *0.40* | *0* | -- | 0 | 0.05 |
| $NO_3$ | *0.55* | *0.07* | *0* | *0.02* | *0.59* | *0* | -- | 0.01 |
| $SO_4$ | *0.17* | *0.24* | *0.07* | *0.25* | *0* | *0.02* | *0* | -- |

The PCA is conducted initially with the whole dataset (N=300), including the hydrochemical composition of natural and artificial snow, water from ponds and groundwater samples. The PCA with clr transformed data shows that only with three principal components, the 87.4 % of total variance can be explained (Fig. 6). The PCA is affected by the presence of natural outliers, in our case from the Na-Cl hydro-facies, that completely distorts the shape of the biplots (Fig. 6B, 6C and 6D). The scores are classified according to the singled out nine water types when considering the complete dataset.

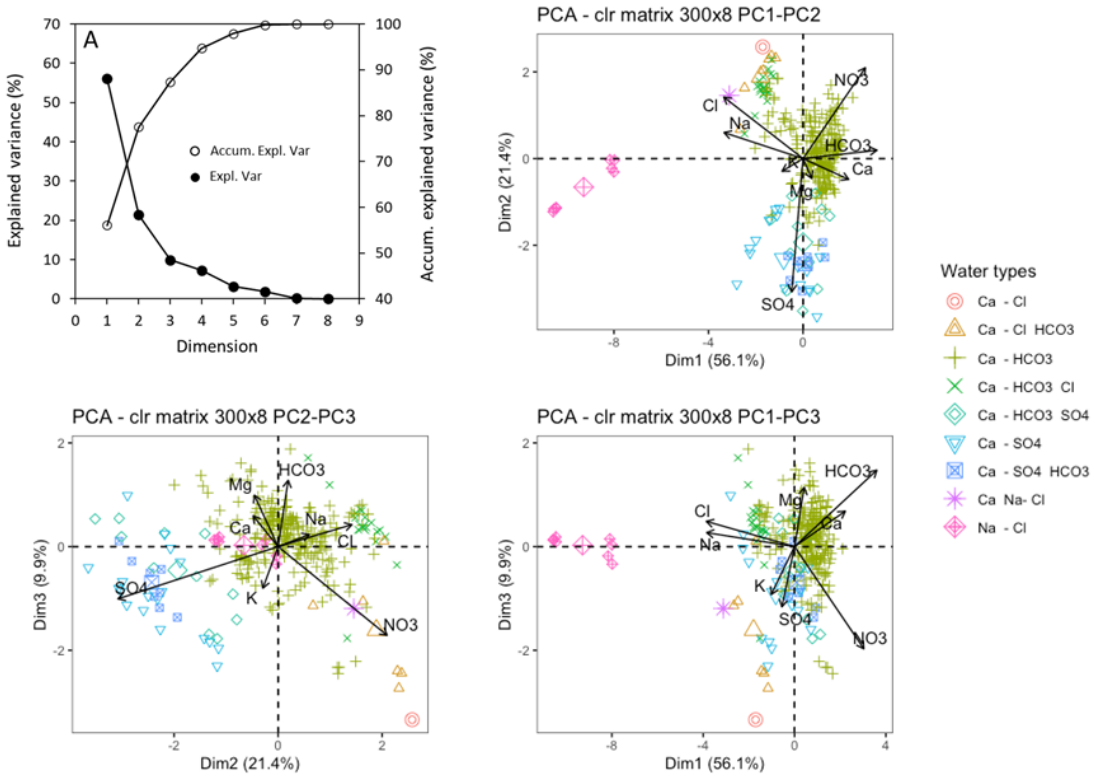


**Fig. 6** (A) Scree-plot of dataset Matrix (300x8) showing the explained (solid circles) variance associated to every PC of the PCA, and the accumulated explained variance (empty circles) as the different PCs are accounted in the PCA. (B) Compositional biplot PC1 vs PC2 (C) Compositional biplot PC2 vs PC3 and (D) Compositional biplot PC1 vs PC3 showing scores (circles) and loadings (arrows) for clr transformed data. In the biplots, the bigger points represent the mean clr-value for each water type.

From the distribution of the water samples in the clr-biplots several subgroups of waters with clear similarities can be read. The biplot between PC2 and PC3 clearly separates sulfate waters. Moreover, looking closely at the biplot between PC1 and PC2 (Fig. 3), different hydrochemical spatial trends can be observed, likely associated with changes in terms of bedrock lithology. In fact, it can be inferred that: (1) The highest clr-variances are shown for $SO_4$, Cl and $NO_3$, followed by Na and $HCO_3$. The lowest clr-variances are shown for Ca, K, and Mg; (2) The PCA has emplaced separately the saltiest waters (M-30 and M-41) in the western quadrant of the biplot. Using clr-transformed data allows to correctly separate characteristic points of the domain, which correspond to the deepest drainage from the Keuper materials; (3) The groundwater samples from the remaining springs are located in the north-eastern and southern quadrants: the freshest waters that are more related to the upper Eocene karst aquifer are situated at the north-eastern

623 quadrant and present some correlation with $NO_3$. The samples related to Cretaceous and
624 Triassic materials appear to be more disperse, being most of them at the south-eastern
625 part of the biplot with extreme values in springs M-21, M-9, M-33, M-36, among others.

626 Taking into account the specific rules for interpreting clr-biplots, the following aspects
627 can be highlighted:

628 - It is possible to draw a link between the vertices of Na, K and Mg, indicating that
629 these variables may form a sub-composition with a single degree of freedom.
630 - The vertices of $SO_4$, Ca and $HCO_3$ lie almost on a common link. This link is also
631 almost orthogonal to the link drawn between Na, K and Mg, suggesting that these
632 two sub-compositions may vary independently of each other.
633 - The two indicated links can be interpreted as two independent set of
634 hydrochemical processes in the springs: (1) The "Pristine Character/Water-Rock
635 interaction" link PCWR [Na, K, Mg] which represents as one end-member, the
636 groundwaters influenced by NaCl contributions derived from Keuper materials
637 but also to recharged waters (Ca–Cl–$HCO_3$; Ca–Cl, Ca–NaCl) at the upper part of
638 the PCM, which represent the other end members of waters that have interacted
639 longer with the Tertiary karst system materials and more evapo-concentrated . (2)
640 The "CARbonate/SULfate dissolution" link 'CARSUL' [$SO_4$, Ca, $HCO_3$]
641 representing the dissolution of different types of carbonate and sulfate rocks
642 ($HCO_3$ as one end member of the link and $SO_4$ as the other one).
643 - Samples in the south-eastern quadrant of the biplot are more disperse and have a
644 stronger association with the $SO_4$ vertices.

645 In the case of the dataset Matrix (43x8) the variation matrix (Table 4) is consistent with
646 that of the dataset Matrix (300x8), showing strong correlations between the same pairs of
647 variables, and even with similar correlation values. The PCA with clr transformed data
648 shows that when considering two or three PCs, 87.4% and 91.7% of total variance can be
649 explained, respectively (Fig. 7). Besides, the resulting clr-biplots are similar in shape to
650 those of Matrix (300x8). As it can be shown, the reduction of the dataset matrices from
651 (300x8) to (43x8) in the PCA does not introduce any relevant change in the final inference
652 regarding the geochemical characteristics of groundwater. This is convenient from the
653 perspective of dimensionality issues.

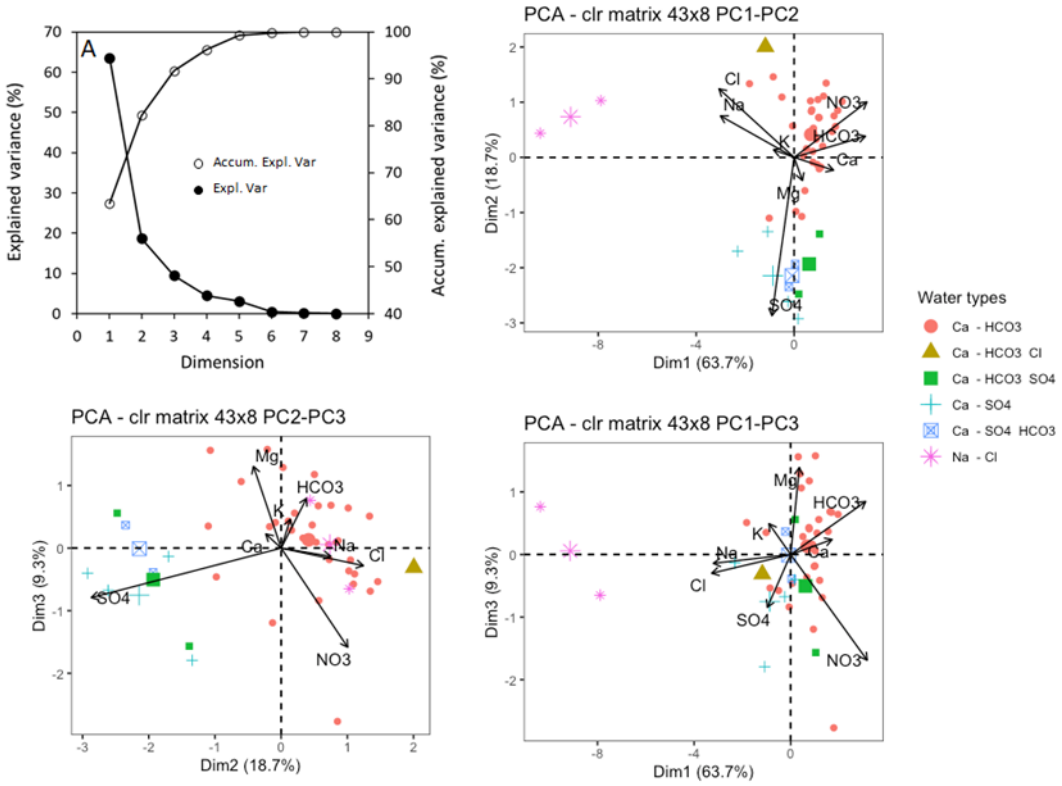


**Fig. 7** (A) Scree-plot of dataset Matrix (43x8) showing the explained variance (solid circles) associated to every PC of the PCA, and the accumulated explained variance (empty circles) as the different PCs are accounted for in the PCA. (B) Compositional biplot PC1 vs PC2 (C) Compositional biplot PC2 vs PC3 and (D) Compositional biplot PC1 vs PC3 showing scores (circles) and loadings (arrows) for clr transformed data. In the biplots, the bigger points represent the mean value for each water type.

### 4.3 Clustering analysis

The GMM clustering analysis was applied to the Matrix (43,8) dataset. Before conducting the ilr transformation, an intuitive sequential binary partition (SBP) was used to characterize the hydrochemical variability within the domain. In this case the partition is based on knowledge of the groundwater chemistry in the study area and on the resulting compositional biplot (Fig 7). As a result, seven groundwater partitions are considered (Table 4): the ilr_1 balance separates the Ca-$HCO_3$ waters (mostly affected by $NO_3$) from the rest; the ilr_2 separates those waters affected/non-affected by $NO_3$ pollution; the ilr_3 separates the contribution of calcite and dolomite to groundwater; the ilr_4 separates Ca

672 from $HCO_3$; the ilr_5 separates $SO_4$ waters from most salty waters; the ilr_6 separates K
673 from Na/Cl; and finally the ilr_7 separates Na and Cl.

674 **Table 4.** SBP of a 7-part composition (ilr_1, ilr_2, …, ilr_7) for describing isometric log
675 ratio (ilr) coordinates based on the separation of anions and cations related to the
676 hydrochemical composition of natural groundwaters for the clustering analysis.
677

| ilr | $Ca^{2+}$ | $Mg^{2+}$ | $Na^{+}$ | $K^{+}$ | $HCO_3^{-}$ | $Cl^{-}$ | $NO_3^{-}$ | $SO_4^{2-}$ |
|---|---|---|---|---|---|---|---|---|
| ilr_1 | +1 | +1 | -1 | -1 | +1 | -1 | +1 | -1 |
| ilr_2 | +1 | +1 | 0 | 0 | +1 | 0 | -1 | 0 |
| ilr_3 | +1 | -1 | 0 | 0 | +1 | 0 | 0 | 0 |
| ilr_4 | +1 | 0 | 0 | 0 | -1 | 0 | 0 | 0 |
| ilr_5 | 0 | 0 | +1 | +1 | 0 | +1 | 0 | -1 |
| ilr_6 | 0 | 0 | +1 | -1 | 0 | +1 | 0 | 0 |
| ilr_7 | 0 | 0 | +1 | 0 | 0 | -1 | 0 | 0 |

678

679 The results obtained from the GMM, suggest that the best multivariate clustering option
680 is obtained applying the 'EEI' model (see Scrucca et al., 2016 for the geometric
681 characteristics of the model) while considering a total of 4 clusters (see Fig. SM.4.1 in
682 Suppl. Mat.).

683 The scatterplot matrix obtained with the model-based clustering process using the seven
684 ilr coordinates, being *D* the previous dimension of the original dataset matrix (43x8), *D*-
685 1 coordinates can be shown in Fig. SM.4.2 (Suppl. Mat.). In order to visualize the clusters
686 in a most suitable way, the dimension reduction function 'MclustDR' (Scrucca, L. 2010)
687 for visualizing the classification structure obtained from the finite mixture of Gaussian
688 densities of the {Mclust} package is used to reduce the dimensionality of the ilr matrix
689 and estimate the principal components. Table. SM.4.1 and Fig. SM.4.3 (Suppl. Mat.)
690 provide the scores of the reduced ilr-matrix and their representation in a scatterplot,
691 respectively. The two main principal components explain 86,42% of the total variance.
692 As a result, with only a glance at the scatterplot of PC1 and PC2 (Fig. 8A) the cluster
693 division for the different springs shows up clearly, and each cluster can be described by
694 the corresponding PDFs (Fig. 8B). It is worth to point out the similarity between the
695 distributions of samples in the 2D space (albeit in a symmetric plane). The Fig. 8C
696 presents the mean hydrochemical composition of each cluster (Table SM.4.2 in Suppl.
697 Mat.) after the modified Stiff diagrams, and Fig. 8D shows in a Piper diagram how the

mean hydrochemical composition of the clusters is representative of the composition of the corresponding springs.

The probabilistic GMM framework estimates the optimal number of clusters and provides for every spring the probability of belonging to these clusters (soft assignment). This approach is more interesting that the classical clustering approaches, in which the number of clusters is assumed fixed, and every spring is assigned to one and only one of the previously assumed clusters (hard assignment) (Kim et al., 2014). From an hydrochemical point of view, the soft assignment often provides the more interesting interpretation because the method reveals if one observation is influenced by several factors (Templ et al., 2008). Moreover, Wu et al., (2017) show how the probabilistic GMM clustering provides insights into hydrochemical processes affecting groundwater, even with a limited number of observations, which is a common situation in high mountain kart aquifers such as the PCM.

The conditional probabilities (P) of assigning one observation to a given cluster (Eq. 7) are given in Table SM.4.3 (Suppl. Mat.). In all cases, springs are assigned to one cluster with a probability > 0.95, and more than 83% of the springs reach the probability of '1'. The smaller probabilities occur in M-01 (P = 0.911 cluster A) and M-13 (P = 0.969 cluster B). Spring M-01 discharges from the Eocene karstic limestones. Nevertheless, this discharge might be affected by weak contributions of Tertiary sulfates (which are related to the formation locally known as 'Beuda gypsum Formation'). The discharge in M-13 shows a Ca-$HCO_3$ hydrogeochemical composition despite discharging from the Triassic (Muschelkalk) limestone aquifer. In this case, the groundwater discharge is weakly affected by the underlying Keuper materials.

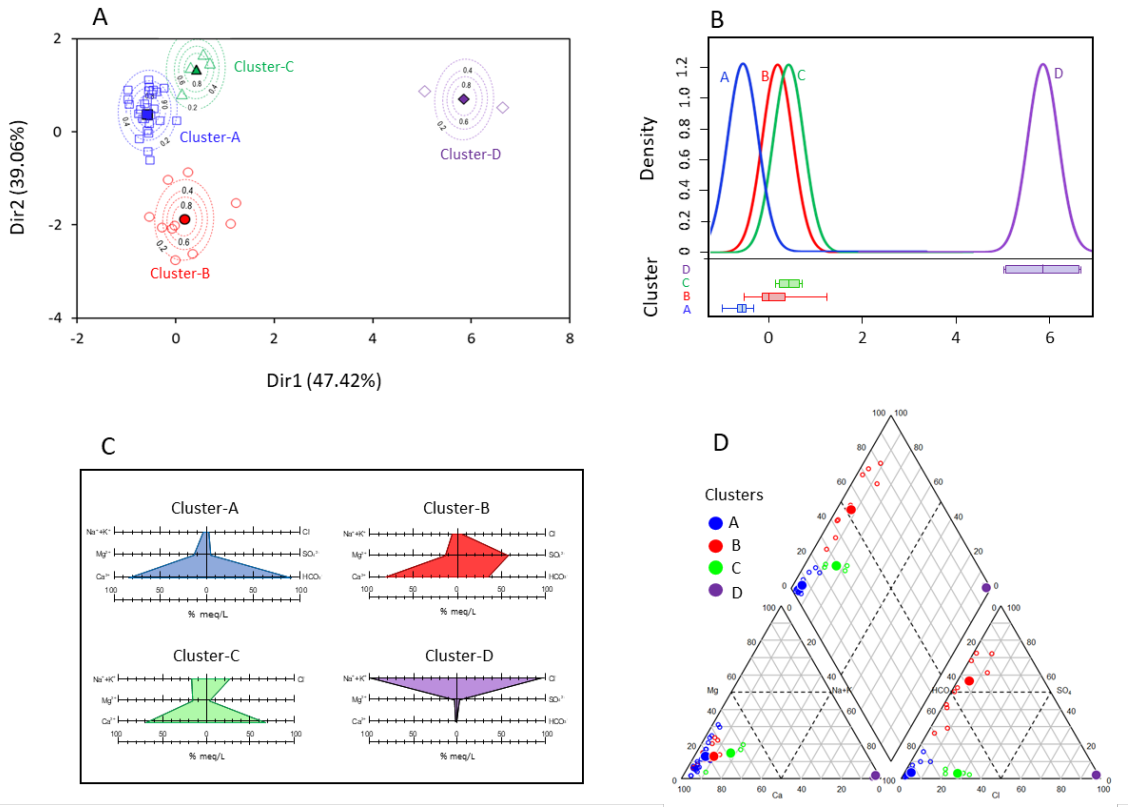


**Fig. 8.** (A) Density biplot for PC1 vs PC2 components obtained from GMM for the Matrix (43x8) of ilr-transformed data after dimension reduction. The dashed lines correspond to the probability zones of belonging a certain cluster in the subspace PC1-PC2. Solid symbols correspond to the mean hydrochemical composition of the clusters. (B) PDF's of the resulting 4 clusters in PC1 (47.42%). (C) Modified Stiff diagram associated to the mean hydrochemical composition of the clusters. (D) Piper diagram associated to the selected springs in the PCM classified by their corresponding cluster to which they belong. Solid symbols correspond to the mean hydrochemical composition of the clusters.

The hydrogeochemical description of each groundwater cluster can be summarized as:

- **Cluster A** is characterized by low mineralization and dominated by slightly alkaline Ca–$HCO_3$ water type. In total 27 springs are grouped in this cluster which correspond to 203 groundwater samples collected in the study from the total of 288. All the springs drain directly or indirectly (i.e. covered by local Quaternary deposits) the Tertiary Eocene upper karst aquifer of the PCM (Fig. 9) and from the higher parts of the mountain (944 - 2144 m a.s.l.). They are mainly found inside the structural limits of the PCM sheet and at its boundaries except some of them localized in Quaternary deposits or discharging karstic conduits trough the

Oligocene carbonate karstic conglomerates situated just in the front of the thrust sheet (e.g. M-03, M-04, M-07, M-39, M-32 and M-43, which is one of the most important karst springs of the system). Another special case is the spring M-06 which lies over Garumnian shales, marls and limestones (Kgp) outcropping materials. In this zone, a fault affecting the stratigraphy might allow the hydrological connection between the lower Eocene limestones (PPEc) and Kgp formations. This connection would explain the Ca–$HCO_3$ water type associated to spring M-06, and also its classification in the cluster A, thus pointing the groundwater discharge origin as the Eocene Tertiary aquifer. Finally, spring M-29 actually drains a Eocene limestone level situated at the west of the PCM boundary.

Cluster A presents the lower EC values, which ranges between 186 and 486 µS/cm and has the minimum values of groundwater temperatures. The concentrations of Cl and $SO_4$ are very low, ranging between 2.5 and 15 mg/L and between 2.6 and 25.3 mg/L respectively. In 13 samples, the concentration of $NO_3$ is above 10 mg/L, and in one specific spring (M-32) it exceeds in all samples the legal limit for potable water (50 mg/L). The average Saturation Indices (SI) estimated with the Phreeqc program (Parkhurst and Appelo, 2013) for calcite, gypsum and halite are 0.23, -2.67 and -9.68, respectively. The groundwaters are representative of the recharge of the karst system in the highest altitudes of the massif, where the dissolution of carbonates is the dominant geochemical process controlling groundwater chemistry.

- **Cluster B** encompasses water types from Ca–$HCO_3$ to Ca–$HCO_3$–$SO_4$, Ca–$SO_4$-$HCO_3$ and Ca–$SO_4$, which are characterized by slightly alkaline moderate mineralization. This group includes 10 springs. A total of 40 groundwater samples collected in the study would correspond to this cluster. The springs related to Cluster B are situated either inside or outside the internal structural limits of the PCM thrust sheet. The springs situated inside (M-9, M-10 and M-13) occur mostly in (1) Cretaceous and Triassic (Keuper) materials outcropping in the area. These materials underly the principal aquifer of the massif (the Eocene carbonate karstic system), and (2) local shallow granular aquifers. The springs M-01, M-02, M-21 and M-36 are related to sediments with high content of Tertiary gypsum from the

Beuda Formation, which outcrops in small pinched out belts located in front of the southeastern part of the PCM thrust sheet. Springs are located at the lowest parts of massif (altitudes ranging between 867 and 1456 m a.s.l.). The EC varies between 493 and 2102 µS/cm. The $SO_4$ concentration is quite high and ranges between 88 and 989 mg/L, exceeding in most cases the legal limit for potable water (250 mg/L). The concentration of Cl ranges between 3.8 and 94.5 mg/L. The average SI for calcite, gypsum and halite are 0.32, -0.99 and - 8.61 respectively.

- **Cluster C** includes water types from Ca–HCO3 and Ca–HCO3-Cl water types. This group includes 4 springs and a total of 37 groundwater samples from which 26 of them correspond to the spring M-20 (located at 1858m a.s.l.). Except the spring M-20, the rest (M-23, M-27, M-42) are located at the boundaries of the PCM geological sheet. The EC varies between 332 and 747 µS/cm. Although they have $SO_4$ concentration similar to cluster A, with 9.7- 15.3 mg/L, the content of Cl is much higher, ranging between 24 and 82 mg/L. These higher values compared to cluster A are interpreted as related with groundwater flow through areas with the presence of relict halite or salty water in closed pores in the Keuper materials, or that may receive the solutes through diffusion. In the case of M-20 (which is located inside the PCM sheet) the salt is related to a klippe of Jurassic delineated into the geological map. Besides, in the catchment area of this spring, there are small outcrops of Keuper materials detected during the fieldwork. The average SI for calcite, gypsum and halite are 0.24, -2.32 and -7.42 respectively.
- **Cluster D** contains the most evident and special waters correspondings to Na–Cl type facies (Fig. 8). This group is composed of 2 salty springs (M-41 and M-30) located at the 993 and 1023 m a.s.l. at the East and West boundaries of the PCM sheet respectively. They are characterized by very high mineralization and saturated in gypsum, discharging from Keuper confined bedrocks and interpreted as the contribution of deep groundwater flow with elevated transit times that allows a significant solute diffusion. The waters are slightly acidic to near-neutral. The M-41 and M-30 samples presents EC values of 57.2 and 247.1 mS/cm, Cl concentrations of 21 and 178.2 g/L, and $SO_4$ concentrations of 1.2 and 8.1 g/L respectively. The M-30 spring can currently be considered the saltiest spring of natural origin in Catalonia as those in the Cardona salt diapire of Oligocene age,

not far away, disappeared due to potash mining activities. Due to the presence of Middle Eocene evaporates at the East boundary of PCM, the M-41 spring can also be affected by an interaction with Tertiary gypsium.

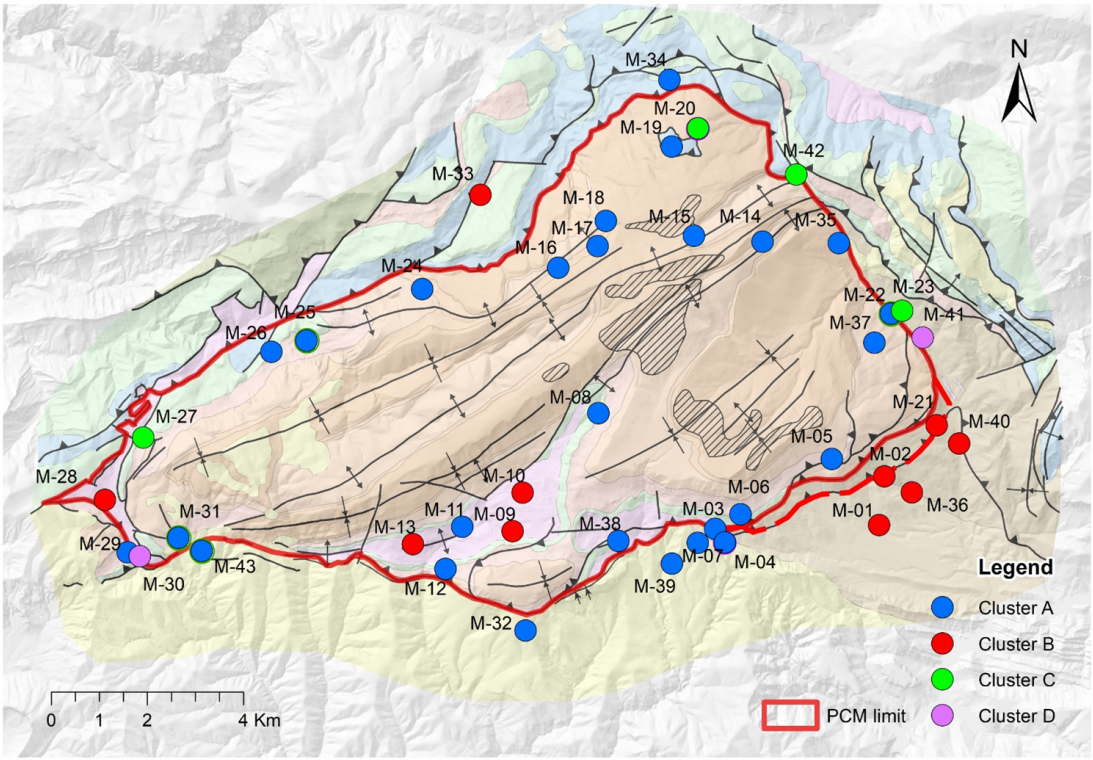


**Fig. 9.** Spatial distributions of the 43 clustered springs over the geological map of the PCM based on the GMM. The description of the different geological materials is the same presented in Fig. 2.

In the framework of multivariate statistics data analysis (e.g. PCA and data clustering), specially dealing with compositional data (i.e. data that carry only information about the relative abundance of each component on the whole, such as the hydrogeochemical data sets), it is important to suitably transform the dataset using the CoDa analysis approach (e.g., Eq.1 or Eq.2) before conducting any analysis. Otherwise it is very likely to obtain wrong results (Otero et al., 2005). Moreover, uninterpretable results are also obtained when applying the classical standardization methodology known as "z-score" on compositional data, which considers logarithms and then subtracts the mean and divides

it by the standard deviation to scale them (Blake et al., 2016). To illustrate the importance of using correct CoDa transformations, the dataset Matrix (43x8) is used to apply the same MSA analysis techniques (PCA and the model-based clustering GMM) but using the classical standardization approach (or z-score normalization). If the effect of the closed nature of the geochemical data is not accounted for, and therefore the CoDa approach is not applyed, then the distribution of loadings (variables) and scores (samples) in the biplots, as well as their interpretation, may be critically affected. In this line, the biplot shown in Fig. SM.5.1. (Suppl. Material) strongly suggests the existence of a negative relationship between all Ca - $HCO_3$ water samples respect all variables, which does not make any hydrogeological sense given the carbonatic nature of the aquifer and the hydrogeological knowledge supporting the existing conceptual model (Herms et al., 2019). Additionally, the clustering results obtained through GMM may have no hydrogeological sense. To illustrate this, Fig. 10 presents the PDF's of the best GMM obtained for PC1 with the dataset Matrix (43x8) from the z-score approach after dimension reduction. Unlike in the case of considering the CoDa approach (Fig. 8B), now the PDFs corresponding to the six clustes identified can not be clearly separated, thus making clustering results uninterpretable.

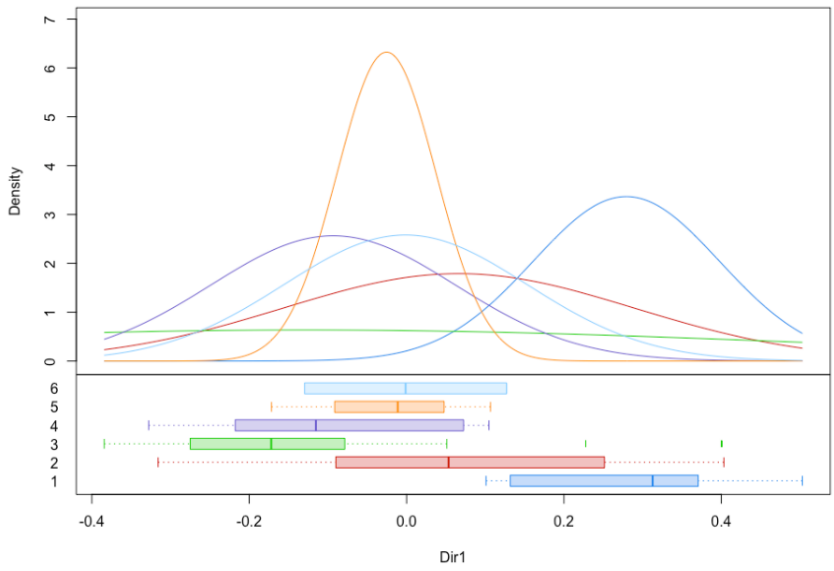


**Fig. 10.** Separated PDF's after dimension reduction with the best GMM with the transformed data using the classical standardization z-score approach.

**4.4 NBLs and TVs values.**

Once the groundwater clusters are defined for the PCM, the NBL and TV's for $NO_3$, $SO_4$ and Cl have been obtained applying the PS-method (Müller et al., 2006). Taking into account the criteria required for data to be accounted when estimating the NBLs with this method (section 3.5), the following observations apply:

- The groundwater samples from M-30 and M-41 (the whole cluster D) present Cl concentrations of geogenic origin above the drinking water limit (>200 mg/L). Therefore, these samples are not considered in the NBL determination.
- $NO_3$ concentrations above the drinking water limit (>50 mg/L) are mostly observed in M-32 spring (cluster A). Besides, the springs M-32, M-10, M-11 and M-28 present $NO_3$ concentrations > 10 mg/L. Following the PS-method criteria, these springs have been excluded of the NBL determination.

The NBLs for the remaining groundwater samples belonging to the clusters A, B and C are obtained taking into account the 90$^{th}$ percentiles (P90) of the corresponding cluster ECDF plots (Fig. 11B). The obtained NBL90 and TVs are presented in Table 5. The results indicate that Tertiary Eocene karst aquifer (cluster A), which is the principal aquifer inside the PCM, presents the lowest NBL90 values for Cl, $SO_4$ and $NO_3$. Cluster B, which is related to the aquifers on the Cretaceous and specially the Triassic Keuper materials, presents the highest NBL90 value for $SO_4$, and Cluster C, which is generally related to local small aquifers located at the boundaries of the PCM, presents the highest values of NBL90 for both Cl and $NO_3$.

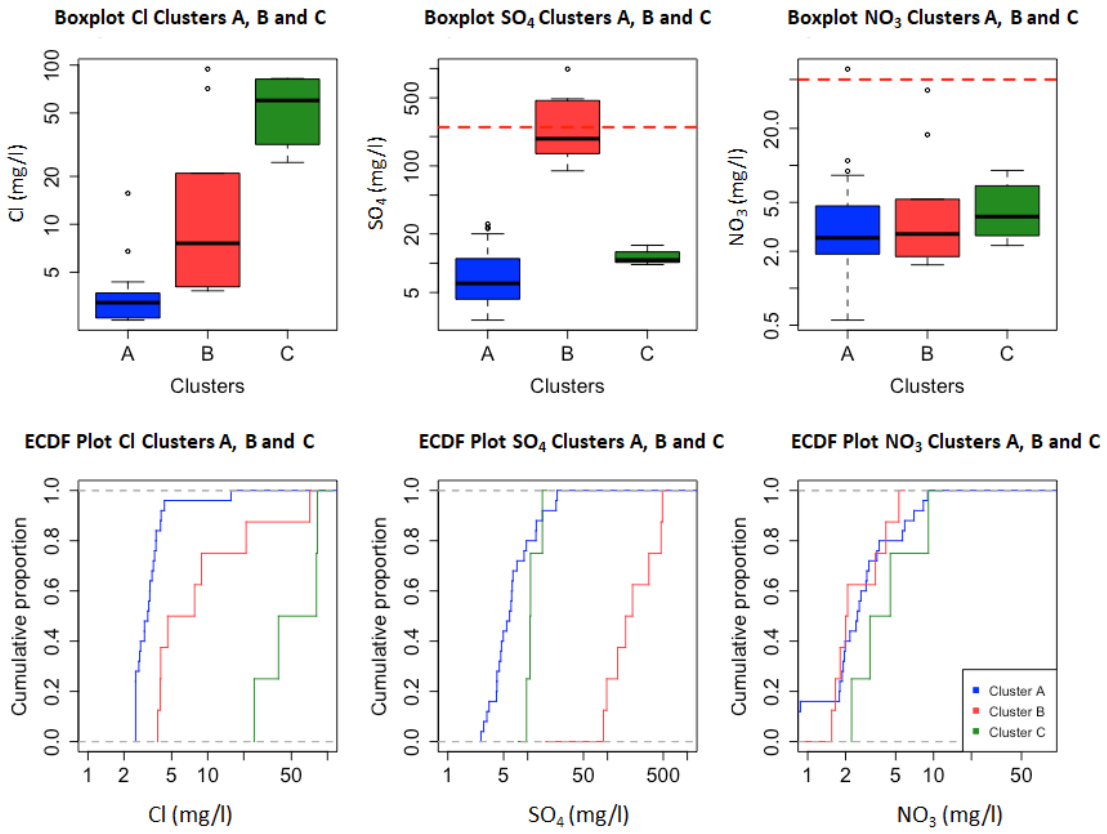


**Fig. 11.** (**A**) boxplots of the clusters A, B and C for $SO_4$, Cl and $NO_3$. The dashed red lines indicate the reference limits established in the Spanish Royal Decree 140/2003 (**B**) ECDF plots.

Comparing the obtained NBL90 values with those officially assigned to GWB-5 and GWB-44 (Table 1), it looks that the NBL official values of $SO_4$ assigned to both GWBs (485 and 609 mg/L, respectively) are likely conditioned by the interaction between fresh groundwater and most probably evaporites of the Upper Triassic (Keuper facies), directly or through diffusion. These evaporites appear very often at the boundaries of many thrust sheets throughout the Southern Pyrenean zone. Additionally, the official NBL90 value of Cl assigned to GWB-44 is similar to that obtained for cluster B, which is related to the Keuper deposits. Likewise, the obtained NBL90 value of $NO_3$ for the Cluster C is similar to the official one for GWB-44. As can be shown, none of the official NBL90 values defined for GWB-5 and GWB-44 correspond to those values obtained for the Lower Eocene limestones and dolomites, which constitute by large the main aquifer of the PCM.

**Table 5.** Summary results of the NBL and TV's values derived from the PS-method (BRIDGE, 2007) for clusters A, B and C for the solutes Cl, $SO_4$ and $NO_3$.

| | Cl [mg/L] | | $SO_4$ [mg/L] | | $NO_3$ [mg/L] | |
|---|---|---|---|---|---|---|
| **Clusters** | **$NBL_{90\%}$** | **TVs** | **$NBL_{90\%}$** | **TVs** | **$NBL_{90\%}$** | **TVs** |
| A | 4.06 ± 2 | 8.12 ± 2 | 14.33 ± 2 | 29.66 ± 2 | 6.55 ± 2 | 13.1 ± 2 |
| B | 35.98 ± 2 | 71.96 ± 2 | 471.71 ± 2 | 471.71 ± 2 | 4.51 ± 2 | 9.02 ± 2 |
| C | 81.92 ± 2 | 140.96 ± 2 | 13.96 ± 2 | 27.92 ± 2 | 7.73 ± 2 | 15.46 ± 2 |

It is well known that high mountain karst aquifers generate highly valuable water resources for the downstream water depending ecosystems. Their protection and rational management is of utmost importance to sustain such ecosystems and satisfying their water demands (Kazakis et al., 2018). In this framework, NBLs provide an objective scale to compare with when the quality status of the aquifer is assessed. Nevertheless, these aquifers are often immersed in deformed and faulted geological structures, as happens in other axial zones of the Central Pyrenees (Lambán et al., 2015), in the Picos de Europa massif (Ballesteros et al., 2015), in the Jura Mountains (Luetscher and Perrin, 2005) and the Hochifen–Gottesacker Alps (Goldscheider, 2005), among others. The NBLs are obtained as a function of the hydrochemical content measured in the different springs discharging the system. Nevertheless, in geological complex zones it is difficult to assert if one certain spring is discharging groundwater from the aquifer of interest or not, because the geographical location of the spring may suggest an origin for the sampled groundwater while hiding mixing relations between groundwater flow lines from other local aquifers with different hydrogeochemical fingerprint (Lambán et al., 2015; Barbieri et al., 2017; Sánchez et al., 2017).

The European Union Water Framework Directive (WFD, 2000) defines a general framework for integrated river basin management in Europe to ensure their "good water status". Nevertheless, the river basin is often an entity hard to manage because the larger the size of the basin the larger is (1) the number of water bodies enclosed and (2) the likelihood of political-administrative boundaries issues to appear. To avoid such problems, instead of looking at river basins, the WFD refocussed on the smaller scale "river basin districts", for which administrative structures were defined to correctly manage the corresponding bodies, thus ensuring -hopefully- the right management of whole river basin (Boeuf and Fritsch, 2016). In this line, the WFD includes the guidelines that apply to define the groundwater bodies (GWB). Even in this case, some scale issues

may arise when considering the definition of the GWB in mountain zones. By definition, the GWB are assumed to belong to a certain river basin. Despite of that, it is well known that groundwater basins, specially in mountain zones, may extend throughout several river basins (Struckmeier et al., 2006; Serianz et al., 2020). As a result, GWBs may include from several aquifers to only parts of them, as it happens in the PCM, whose discharge contributes to both the Ebro and the Llobregat rivers through GWB-44 and GWB-5, respectively. This is the reason why there are two different sets of NBL applying for the same aquifer (Table 1).

The WFD recognises the importance of having well defined NBLs. Given that these values are used to quantitatively assess whether or not anthropogenic pollution is taking place in the corresponding aquifer (Nieto et al., 2005), their characterization must be based on (1) a consistent and rigorous hydrochemical criteria, and (2) a sound hydrogeological conceptual model. The hydrogeological fingerprint of each aquifer belonging to the same GWB may be different. Therefore, the criterion of defining a single set of NBLs for the whole GWB may have no sense. Moreover, such criterium may be counterproductive from a safety perspective, given that one may assume for the GWB some concentrations of species or chemical substances present in solution as normal, when actually those concentrations may be already indicating the existence of a polluting issue in some aquifers of the GWB. This is even worst when only one of these aquifers play a relevant role from a water resources perspective, as happens in the PCM. Here, the Lower Eocene karst aquifer generates an overall mean groundwater discharge that represents 15% of the mean annual water consumption in the city of Barcelona (Herms et al., 2019). Therefore, from a water resources management perspective, it might worth defining NBLs at the local scale for each aquifer. In this line, the methodology presented in this work to "complement" the sample pre-selection method is a useful tool to objectively reel off the NBL of the different high mountain aquifers belonging to a given GWB. Besides, the proposed methodology provides the GWBs managing authorities a full-sense hydrochemical criteria to better protect the high mountain pristine and strategic aquifers, while ensuring the good status of the associated high mountain river basins.

# 5. Conclusions

The PCM is a complex hydrogeological system composed by a main Eocene karst aquifer that drives the hydrodynamical discharge response of the massif. The PCM also includes small aquifers whose discharge present a different hydrochemical composition. The discrepancies between the official NBLs of the GWBs associated to the PCM reveal the disparities in the hydrochemical composition of groundwater from the different sampled springs belonging the GWBs. To estimate correctly the NBLs associated to one aquifer it is necessary to consider only samples from springs discharging groundwater from the aquifer of interest. In high complex hydrogeological settings, this selection is not easy and must be guided by a consistent and objective clustering method.

In the case of the PCM, four compositional groups have been identified by means of GMM clustering analysis. Most of the analysed springs are dominated by Ca–$HCO_3$ water type coming from the main aquifer of the area. There are some springs dominated by Ca–$HCO_3$, Ca–$HCO_3$–$SO_4$, Ca–$SO_4$-$HCO_3$, Ca–$SO_4$, Ca–$HCO_3$-Cl, Na–Cl water types derived from other small/local aquifers. Determination of NBLs values in the area must take into account the four groups defined in this study.

In complex aquifer systems, the proposed soft clustering approach, which is based on probabilistic Gaussian mixture models, provides the optimal number of clusters for the sampled springs only based upon the observed compositional data, while estimating the probability of belonging to everyone of these clusters for each spring. The presented clustering approach relies on multivariate statistics methods. In this framework, it is essential to transform the dataset using the CoDa analysis rules, specially when dealing with hydrochemical compositions. Otherwise, uninterpretable results will be likely obtained.

In the case of different existing aquifers with discrepant hydrochemical fingerprints in the same GWBs, it would be reasonable to evaluate the NBLs in all of them rather than having a single set of NBLs for the whole GWB. Otherwise, errors may appear when estimating the quality status of some of these aquifers, even if the overall assessed quality status of the GWB appears to be correct.

## Acknowledgements:

This research has been supported by Agencia Estatal de Investigación (AEI) from the Spanish Government and the European Regional Development Fund (FEDER) from EU through PACE-ISOTEC (CGL2017-87216-C4-1-R) projects, the EFA210/16/ PIRAGUA project which is co-founded by the European Regional Development Fund (ERDF) through the Interreg V Spain-France-Andorre Programme (POCTEFA 2014-2020) of the European Union, the Catalan Government projects to support consolidated research groups MAG (Mineralogia Aplicada, Geoquimica i Geomicrobiologia, 2017SGR-1733) from Universitat de Barcelona (UB) and GREM (Grup de Recerca de Minería Sostenible) from the Universidades Universitat Politècnica de Catalunya (UPC), the Ministerio de Ciencia, Innovación y through the METhods for COmpositional analysis of DAta (CODAMET) project (Ref: RTI2018-095518-B-C22, 2019-2021). We thank the Hydrogeology and Geothermics Unit Team of the Institut Cartogràfic i Geològic de Catalunya (ICGC) by their helpful collaboration. We acknowledge the Confederacion Hidrográfica del Ebro (CHE) and Agència Catalana de l'Aigua (ACA) for providing the official NBLs for WGB44 and WGB5, respectively. Meteorological data have been kindly provided by the Spanish Meteorological Agency (AEMET) and the Meteorological Service of Catalonia (SMC).


## References


Aitchison, J., 1986. The Statistical Analysis of Compositional Data. Monographs on Statistics and Applied Probability Chapman and Hall, London, New York (416 pp.).

Aitchison, J., Greenacre, M., 2002. Biplots of compositional data. Journal of the Royal Statistical Society: Series C (Applied Statistics), 51(4), 375–392. doi:10.1111/1467-9876.00275

Appelo, C., Postma, D., 2005. Geochemistry, Groundwater and Pollution. 2nd edition. London: CRC Press, 683 pp. https://doi.org/10.1201/9781439833544

Ballesteros, D., Malard, A., Jeannin, P. Y., Jiménez-Sánchez, M., García-Sansegundo, J., Meléndez-Asensio, M., Sendra, G., 2015. KARSYS hydrogeological 3D modeling of alpine karst aquifers developed in geologically complex areas: Picos de Europa National Park (Spain). Environmental Earth Sciences, 74(12), 7699-7714. https://doi.org/10.1007/s12665-015-4712-0

1016 Barbieri, M., Nigro, A., Petitta, M., 2017. Groundwater mixing in the discharge area of
1017 San Vittorino Plain (Central Italy): geochemical characterization and implication
1018 for drinking uses. Environmental Earth Sciences, 76(11), 393.
1019 https://doi.org/10.1007/s12665-017-6719-1
1020 Biernacki, C., Govaert, Gérard., 1999. Choosing models in model-based clustering and
1021 discriminant analysis. J. Stat. Comput. Simul. 64, 49–71.
1022 https://doi.org/10.1080/00949659908811966
1023 Blake, S., Henry, T., Murray, J., Flood, R., Muller, M.R., Jones, A.G., Rath, V., 2016.
1024 Compositional multivariate statistical analysis of thermal groundwater provenance:
1025 A hydrogeochemical case study from Ireland. Appl. Geochem. 75, 171–188.
1026 https://doi.org/10.1016/j.apgeochem.2016.05.008
1027 Boeuf, B., Fritsch, O., 2016. Studying the implementation of the Water Framework
1028 Directive in Europe: a meta-analysis of 89 journal articles. Ecology and Society,
1029 21(2):19. http://dx.doi.org/10.5751/ES-08411-210219
1030 Bondu, R., Cloutier, V., Rosa, E., Roy, M., 2020. An exploratory data analysis approach
1031 for assessing the sources and distribution of naturally occurring contaminants (F,
1032 Ba, Mn, As) in groundwater from southern Quebec (Canada). Appl. Geochem. 114,
1033 104500. https://doi.org/10.1016/j.apgeochem.2019.104500
1034 Bouveyron, C., Brunet-Saumard, C., 2014. Model-based clustering of high-dimensional
1035 data: A review. Comput. Stat. Data Anal. 71, 52–78.
1036 https://doi.org/10.1016/j.csda.2012.12.008
1037 BRIDGE, 2007. Background cRiteria for the IDentification of Groundwater Thresholds.
1038 https://cordis.europa.eu/project/id/6538.
1039 Brock, G., Pihur, V., Datta, S., Datta, S., 2008. clValid: An R Package for Cluster
1040 Validation. Journal of Statistical Software 25(4). doi: 10.18637/jss.v025.i04
1041 Buccianti, A., Grunsky, E., 2014. Compositional data analysis in geochemistry: Are we
1042 sure to see what really occurs during natural processes? J. Geochem. Explor. 141,
1043 1–5. https://doi.org/10.1016/j.gexplo.2014.03.022
1044 Buccianti, A., Lima, A., Albanese, S., De Vivo, B., 2018. Measuring the change under
1045 compositional data analysis (CoDA): Insight on the dynamics of geochemical
1046 systems. J. Geochem. Explor. 189, 100–108.
1047 https://doi.org/10.1016/j.gexplo.2017.05.006

Carranza, E.J.M., 2011. Analysis and mapping of geochemical anomalies using logratio-transformed stream sediment data with censored values. J. Geochem. Explor. 110, 167–185. https://doi.org/10.1016/j.gexplo.2011.05.007

Charrad, M., Ghazzali, N., Boiteau, V., Niknafs, A., 2014. NbClust: an R package for determining the relevant number of clusters in data set. J Stat Soft.61:1–36.

Cloutier, V., Lefebvre, R., Therrien, R., Savard, M.M., 2008. Multivariate statistical analysis of geochemical data as indicative of the hydrogeochemical evolution of groundwater in a sedimentary rock aquifer system. J. Hydrol. 353, 294–313. https://doi.org/10.1016/j.jhydrol.2008.02.015

Coetsiers, M., Blaser, P., Martens, K., Walraevens, K., 2009. Natural background levels and threshold values for groundwater in fluvial Pleistocene and Tertiary marine aquifers in Flanders, Belgium. Environ. Geol. 57, 1155–1168. https://doi.org/10.1007/s00254-008-1412-z

Comas-Cufí, M., Thió-Henestrosa, S., 2011. CoDaPack 2.0: a stand-alone, multi-platform compositional software. In: Egozcue JJ, Tolosana-Delgado R, Ortego MI, eds. CoDaWork'11: 4th International Workshop on Compositional Data Analysis. Sant Feliu de Guíxols.

Custodio, E.; Nieto, P.; Manzano, M., 2007. Natural groundwater quality: policy considerations and European opinion.The Natural Baseline Quality of Groundwater (eds. W.M. Edmunds & P. Shand). Blackwell Publ., Oxford. Chap. 8: 178–194. ISBN: 978–14051–5675–2.Dempster, A. P. , Laird, N. M.; Rubin, D. B. 1977. Maximum Likelihood from Incomplete Data via the EM Algorithm. Journal of the Royal Statistical Society. Series B (Methodological), Vol. 39, No. 1. pp. 1-38. DOI: 10.2307/2984875

Drew, D., Hötzl, H. (eds.), 1999. Karst Hydrogeology and Human Activities. Impacts, Consequences and Implications. – International Contributions to hydrogeology (IAH) 20, 322 p.

Ducci, D., Sellerino, M., 2012. Natural background levels for some ions in groundwater of the Campania region (southern Italy). Environ. Earth Sci. 67, 683–693. https://doi.org/10.1007/s12665-011-1516-8

Egozcue, J., Pawlowsky-Glahn, V., Mateu-Figueras, F., Barceló-Vidal, C., 2003. Isometric logratio transformations for compositional data analysis. Math Geol;35:279–300.

1081 Egozcue, J.J. Pawlowsky-Glahn, V., 2005. Groups of parts and their balances in
1082 compositional data analysis. Mathematical Geology, 37(7), 795-828.
1083 Egozcue, J., Pawlowsky-Glahn V., 2006. Simplicial geometry for compositional data. In:
1084 Buccianti A, Mateu-Figueros G, Pawlowsky-Glahn V, editors. Compositional data
1085 analysis in the geosciences: from theory to practice. Bath, UK: Geological Society
1086 Publishing House; p. 67–77.
1087 Engle, M.A., Rowan, E.L., 2013. Interpretation of Na–Cl–Br Systematics in Sedimentary
1088 Basin Brines: Comparison of Concentration, Element Ratio, and Isometric Log-
1089 ratio Approaches, Math Geosci (2013) 45:87-101 DOI 10.1007/s11004-012-9436-
1090 z
1091 Farnham, I.M., Sinh, A.k., Stetzenbach, K.J., Johannesson, K.H., 2002. Treatment of
1092 nondetects in multivariate analysis of groundwater geochemistry data.
1093 Chemometrics and Intelligent Laboratory Systems. Volume 60, Issues 1–2, 28 pp
1094 265-281. https://doi.org/10.1016/S0169-7439(01)00201-5
1095 Filzmoser, P., Steiger, B., 2009. StatDA: statistical analysis for environmantel data. R
1096 package version 1.1. http://cran.at.r-project.org/web/packages/StatDA/index.html.
1097 Filzmoser, P., Hron, K., Reimann, C., 2009b. Univariate statistical analysis of
1098 environmental (compositional) data: problems and possibilities. Sci Total Environ
1099 407:6100–8. https://doi.org/10.1016/j.scitotenv.2009.08.008
1100 Filzmoser, P., Hron, K., Templ, M., 2018. Applied Compositional Data Analysis. With
1101 Worked Examples in R. Springer Series in Statistics. doi:10.1007/978-3-319-
1102 96422-5
1103 Fraley, C., Raftery, A.E., 2002. Model-based clustering, discriminant analysis and density
1104 estimation, Journal of the American Statistical Association, 97/458, pp. 611-631
1105 Fraley, C., Raftery, A.E., Murphy, T.B., Scrucca, L., 2012. mclust Version 4 for R:
1106 Normal Mixture Modeling for Model-Based Clustering, Classification, and Density
1107 Estimation. Technical Report No. 597, Department of Statistics, University of
1108 Washington
1109 Gabriel, K.R., 1971. The biplot-graphic display of matrices with application to principal
1110 component analysis. Biometrika 58, 453e467.
1111 Goldscheider, N., 2005. Fold structure and underground drainage pattern in the alpine
1112 karst system Hochifen-Gottesacker. Eclogae geol. Helv. 98, 1–17.
1113 https://doi.org/10.1007/s00015-005-1143-z

Güller, C., Thyne, G.D., 2004. Delineation of hydrochemical facies distribution in a regional groundwater system by means of fuzzy c-means clustering. Water Resour Res 40:W12503. https://doi.org/10.1029/2004WR003299

He Kim, S.H., Choi, B., Lee, G., Yun, S., Kim S., 2019. Compositional data analysis and geochemical modeling of CO2–water–rock interactions in three provinces of Korea. Environ Geochem Health 41, 357–380. https://doi.org/10.1007/s10653-017-0057-9

Herms, I., Jódar, J., Soler, A., Vadillo, I., Lambán, L. J., Martos-Rosillo, S., Núñez, J.A., Arnó, G., Jorge, J., 2019. Contribution of isotopic research techniques to characterize high-mountain-Mediterranean karst aquifers: The Port del Comte (Eastern Pyrenees) aquifer. Science of The Total Environment, 656, 209-230. https://doi.org/10.1016/j.scitotenv.2018.11.188

Hinsby, K., Condesso de Melo, M.T., Dahl, M., 2008. European case studies supporting the derivation of natural background levels and groundwater threshold values for the protection of dependent ecosystems and human health. Sci. Total Environ. 401, 1–20. https://doi.org/10.1016/j.scitotenv.2008.03.018

ICGC, 2007. Mapa Geològic Comarcal de Catalunya 1:50,000. Full Alt Urgell (BDGC50M).http://www.icgc.cat/ca/Administracio-i-empresa/Descarregues/Cartografia-geologica-i-geotematica/Cartografia-geologica/Mapa-geologic-comarcal-de-Catalunya-1-50.000/Mapa-geologic-comarcal-de-Catalunya-1-50.000.

Kassambara, A., Mundt, F., 2016. Package 'factoextra': Extract and Visualize the Results of Multivariate Data Analyses, https://CRAN.R-project.org/package=factoextra, r package version 1.0.3.

Kazakis, N., Chalikakis, K., Mazzilli, N., Ollivier, C., Manakos, A., Voudouris, K., 2018. Management and research strategies of karst aquifers in Greece: Literature overview and exemplification based on hydrodynamic modelling and vulnerability assessment of a strategic karst aquifer, Sci. Total Environ. 643, 592-609, https://doi.org/10.1016/j.scitotenv.2018.06.184.

Kim, K.-H., Yun, S.-T., Park, S.-S., Joo, Y., Kim, T.-S., 2014. Model-based clustering of hydrochemical data to demarcate natural versus human impacts on bedrock groundwater quality in rural areas, South Korea. J. Hydrol. 519, 626–636. https://doi.org/10.1016/j.jhydrol.2014.07.055

1147 Kim, K.-H., Yun, S.-T., Kim, H.-K., Kim, J.-W., 2015. Determination of natural
1148 backgrounds and thresholds of nitrate in South Korean groundwater using model-
1149 based statistical approaches. J. Geochem. Explor. 148, 196–205.
1150 https://doi.org/10.1016/j.gexplo.2014.10.001
1151 Kresic, N., Stevanović, Z., 2010. Groundwater hydrology of springs: engineering, theory,
1152 management, and sustainability. Butterworth-Heinemann, Oxford
1153 Kürzl, H., 1988. 'Exploratory data analysis: recent advances for the interpretation of
1154 geochemical data. Journal of Geochemical Exploration, 30(1-3), 309–322.
1155 https://doi.org/10.1016/0375-6742(88)90066-0
1156 Lambán, L.J., Jódar, J., Custodio, E., Soler, A., Sapriza, G., Soto, R., 2015. Isotopic and
1157 hydrogeochemical characterization of high-altitude karst aquifers in complex
1158 geological settings. The Ordesa and Monte Perdido National Park (Northern Spain)
1159 case study. Science of the Total Environment, 506, 466-479.
1160 http://dx.doi.org/10.1016/j.scitotenv.2014.11.030
1161 Luetscher, M., Perrin, J., 2005. The Aubonne karst aquifer (Swiss Jura). Eclogae
1162 Geologicae Helvetiae, 98(2), 237-248. https://doi.org/10.1007/s00015-005-1156-7
1163 Marandi, A., Karro, E., 2008. Natural background levels and threshold values of
1164 monitored parameters in the Cambrian-Vendian groundwater body, Estonia.
1165 Environ. Geol. 54, 1217–1225. https://doi.org/10.1007/s00254-007-0904-6
1166 Marín, A.I., Andreo, B., 2015. Vulnerability to Contamination of Karst Aquifers. In:
1167 Stevanović Z. (eds) Karst Aquifers—Characterization and Engineering.
1168 Professional Practice in Earth Sciences. Springer, Cham.
1169 https://doi.org/10.1007/978-3-319-12850-4_8
1170 Martín-Fernández, J.A., Barceló-Vidal, C., Pawlowsky-Glahn, V., 2003. Dealing with
1171 zeros and missing values in compositional data sets using nonparametric
1172 imputation. Mathematical Geology 35 (3), 253–278.
1173 Merchán, D., Auqué, L.F., Acero, P., Gimeno, M.J., Causapé, J., 2015. Geochemical
1174 processes controlling water salinization in an irrigated basin in Spain: Identification
1175 of natural and anthropogenic influence. Sci. Total Environ. 502, 330–343.
1176 https://doi.org/10.1016/j.scitotenv.2014.09.041
1177 MHCASWS, 2003. Royal Decree 140/2003 of 7 February by which health criteria for the
1178 quality of water intended for human consumption are established. Ministry of
1179 Health, Consumer Affairs and Social Welfare, Spain

Moya, C.E., Raiber, M., Taulis, M., Cox, M.E., 2015. Hydrochemical evolution and groundwater flow processes in the Galilee and Eromanga basins, Great Artesian Basin, Australia: A multivariate statistical approach. Sci. Total Environ. 508, 411–426. https://doi.org/10.1016/j.scitotenv.2014.11.099

Müller, D., Blum, A., Hart, A., Hookey, J., Kunkel, R., Scheidleder, A., Tomlin, C., Wendland, F., 2006. Final proposal for a methodology to set up groundwater threshold values in Europe. In: Report to the EU project ‘‘BRIDGE’’, Deliverable D18.

Muñoz, J.A., Mencos, J., Roca, E., Carrera, N., Gratacós, A., Ferrer, O. Fernández, O., 2018. The structure of the South-Central-Pyrenean fold and thrust belt as constrained by subsurface data. Geologica Acta, Vol.16, No 4, 439-460 DOI: 10.1344/GeologicaActa2018.16.4.7

Nieto, P., Custodio, E., Manzano, M., 2005. Baseline groundwater quality: a European approach. Environmental Science & Policy, 8(4), 399-409. https://doi.org/10.1016/j.envsci.2005.04.004

Otero, N., Tolosana-Delgado, R., Soler, A., Pawlowsky-Glahn, V., Canals, A., 2005. Relative vs. absolute statistical analysis of compositions: A comparative study of surface waters of a Mediterranean river. Water Res. 39, 1404–1414. https://doi.org/10.1016/j.watres.2005.01.012

Owen, D.Des.R., Pawlowsky-Glahn, V., Egozcue, J.J., Buccianti, A., Bradd, J.M., 2016. Compositional data analysis as a robust tool to delineate hydrochemical facies within and between gas-bearing aquifers: COMPOSITIONAL DATA ANALYSIS TO DELINEATE WATER TYPES. Water Resour. Res. 52, 5771–5793. https://doi.org/10.1002/2015WR018386

Palarea-Albaladejo, J., Martin-Fernandez, J.A., Olea, R.A.,2014. A bootstrap estimation scheme for chemical compositional data with nondetects. Journal of Chemometrics, 28: 585-599. https://doi.org/10.1002/cem.2621

Palarea-Albaladejo, J., Martin-Fernandez, J.A., 2015. zCompositions — R package for multivariate imputation of left-censored data under a compositional approach. Chemometrics and Intelligent Laboratory Systems, Volume 143, pp 85-96, ISSN 0169-7439, https://doi.org/10.1016/j.chemolab.2015.02.019.

Parkhurst, D.L., Appelo, C.A.J., 2013. Description of Input and Examples for PHREEQC Version 3—A Computer Program for Speciation, Batch-Reaction, One-Dimensional Transport, and Inverse Geochemical Calculations: U.S. Geological

Survey Techniques and Methods, Book 6, Chap. A43: 1–497. (Available only at https://pubs.usgs.gov/tm/06/a43. Last access 28 August 2020).

Parrone, D., Ghergo, S., Preziosi, E., 2019. A multi-method approach for the assessment of natural background levels in groundwater. Sci. Total Environ. 659, 884–894. https://doi.org/10.1016/j.scitotenv.2018.12.350

Pawlowsky-Glahn, V., Egozcue, J.J., Tolosana-Delgado, R., 2015. Modeling and Analysis of Compositional Data. ed. John Wiley & Sons Ltd, The Atrium, Southern Gate, Chichester, West Sussex, PO19 8SQ, United Kingdom. 272 pages. ISBN: 9781118443064

Peel, M.C., Finlayson, B.L., McMahon, T.A., 2007. Updated world map of the Köppen–Geiger climate classification. Hydrol. Earth Syst. Sci. 11, 1633–1644. https://doi.org/ 10.5194/hess-11-1633-2007.

Piña, A., Donado, L.D., Blake, S., Cramer, T., 2018. Compositional multivariate statistical analysis of the hydrogeochemical processes in a fractured massif: La Línea tunnel project, Colombia. Appl. Geochem. 95, 1–18. https://doi.org/10.1016/j.apgeochem.2018.05.012

Preziosi, E., Giuliano, G., Vivona, R., 2010. Natural background levels and threshold values derivation for naturally As, V and F rich groundwater bodies: a methodological case study in Central Italy. Environ. Earth Sci. 61, 885–897. https://doi.org/10.1007/s12665-009-0404-y

Puig, R., Tolosana-Delgado, R., Otero, N., Folch, A., 2011. Combining isotopic and compositional data: a discrimination of regions prone to nitrate pollution. In V. Pawlowsky-Glahn and A. Buccianti (Eds.), Compositional Data Analysis: Theory and Applications 390.

Raftery, AE., Scrucca, L., Brendan, T., Fop, M., 2020. Gaussian Mixture Modelling for Model-Based Clustering, Classification, and Density Estimation. Package 'mclust'. Version 5.4.6. https://mclust-org.github.io/mclust/

Reimann, C., Filzmoser, P., 2000. Normal and lognormal data distribution in geochemistry: death of a myth. Consequences for the statistical treatment of geochemical and environmental data. Environmental Geology 39, 1001–1014. https://doi.org/10.1007/s002549900081

Reimann, C., Filzmoser, P., Garrett, R.G., Dutter, R., 2008. Statistical data analysis explained. Applied environmental statistics with R. Wiley, Chichester, UK, 362 pp. ISBN: 978-0-470-98581-6

1248 Reimann, C., Filzmoser, P., Fabian, K., Hron, K., Birke, M., Demetriades, A., Dinelli, E.,
1249 Ladenberger, A., 2012. The concept of compositional data analysis in practice —
1250 Total major element concentrations in agricultural and grazing land soils of Europe.
1251 Sci. Total Environ. 426, 196–210. https://doi.org/10.1016/j.scitotenv.2012.02.032
1252 Sánchez, D., Antonio Barberá, J., Mudarra, M., Andreo, B., Martín, J.F., 2017.
1253 Hydrochemical and isotopic characterization of carbonate aquifers under natural
1254 flow conditions, Sierra Grazalema Natural Park, southern Spain. Geological
1255 Society, London, Special Publications, 466(1), 275–293. doi:10.1144/sp466.16
1256 Scrucca, L., 2010. Dimension reduction for model-based clustering. Statistics and
1257 Computing, 20(4), pp. 471-484.
1258 Scrucca, L., Fop, M., Murphy, T.B., Raftery, A.E., 2016. Mclust 5: clustering,
1259 classification and density estimation using Gaussian finite mixture models, The R
1260 Journal, 8/1, pp. 289-317.
1261 Serianz, L., Cerar, S. Šraj, M., 2020. Hydrogeochemical characterization and
1262 determination of natural background levels (NBL) in groundwater within the main
1263 lithological units in Slovenia. Environ Earth Sci 79, 373.
1264 https://doi.org/10.1007/s12665-020-09112-1
1265 Shelton, J.L., Engle, M.A., Buccianti, A., Blondes, M.S., 2018. The isometric log-ratio
1266 (ilr)-ion plot: A proposed alternative to the Piper diagram. J. Geochem. Explor. 190,
1267 130–141. https://doi.org/10.1016/j.gexplo.2018.03.003
1268 Stevanović, Z., 2019. Karst waters in potable water supply: a global scale overview.
1269 Environ Earth Sci 78, 662. https://doi.org/10.1007/s12665-019-8670-9
1270 Struckmeier, W.F., Gilbrich, W.H., Gun, J.v.d., Maurer, S., Puri, S., Richts, A., Winter,
1271 P., Zaepke, M., 2006. WHYMAP and the groundwater resources map of the world
1272 at the scale of 1:50 000 000. Special edition for the 4th world water forum, Mexico
1273 City, March 2006. BGR Hannover/UNESCO, Paris.
1274 Suk, H., Lee, K.K., 1999. Characterization of a groundwater hydrochemical system
1275 through multivariate analysis: clustering into groundwater zones. Groundwater v.
1276 37, no. 3pp. 358-366.
1277 Templ, M., Filzmoser, P., Reimann, C., 2008. Cluster analysis applied to regional
1278 geochemical data: Problems and possibilities. Appl. Geochem. 23, 2198–2213.
1279 https://doi.org/10.1016/j.apgeochem.2008.03.004
1280 Tolosana-Delgado, R., Otero, N., Soler, A., 2005. A compositional approach to stable
1281 isotope data analysis. Conference: CODAWORK'05

Van den Boogaart, K.G. Tolosana-Delgado, R., 2008 ”Compositions”: a unified R package to analyze Compositional Data, Computers & Geosciences. 34 (4), 320-338. https://doi.org/10.1016/j.cageo.2006.11.017

Vergés, J., 1999. Estudi geològic del vessant sud del Pirineu oriental i central. Evolució cinemàtica en 3D. PhD Thesis. University of Barcelona (UB), Faculty of Geology, 180 pp.

Viviroli, D., Kummu, M., Meybeck, M., Kallio, M., Wada, Y., 2020. Increasing dependence of lowland populations on mountain water resources. Nature Sustainability, 1-12. https://doi.org/10.1038/s41893-020-0559-9

Wendland, F., Blum, A., Coetsiers, M., Gorova, R., Griffioen, J., Grima, J., Hinsby, K., Kunkel, R., Marandi, A., Melo, T., Panagopoulos, A., Pauwels, H., Ruisi, M., Traversa, P., Vermooten, J.S.A., Walraevens, K., 2008. European aquifer typology: a practical framework for an overview of major groundwater composition at European scale. Environ. Geol. 55, 77–85. https://doi.org/10.1007/s00254-007-0966-5

WFD, 2000. Water Framework Directive, 2000. Directive 2000/60/CE of the European Parliament (ECOJ 22 December 2000). http://www.bygg.ntnu.no/borsanyi/eamn_web/documents/wfd-es.pdf.

Wu, X., Zheng, Y., Zhang, J., Wu, B., Wang, S., Tian, Y., Li, J., Meng, X., 2017. Investigating Hydrochemical Groundwater Processes in an Inland Agricultural Area with Limited Data: A Clustering Approach. Water 9, 723. https://doi.org/10.3390/w9090723

Yidana, S.M., 2010. Groundwater classification using multivariate statistical methods: Southern Ghana. Journal of African Earth Sciences 57(5):455-469 doi: 10.1016/j.jafrearsci.2009.12.002

Yolcubal, İ., Gündüz, Ö.C.A., Kurtuluş, N., 2019. Origin of salinization and pollution sources and geochemical processes in urban coastal aquifer (Kocaeli, NW Turkey). Environmental Earth Sciences, 78(6), 181. https://doi.org/10.1007/s12665-019-8181-8

Zabala, M.E., Martínez, S., Manzano, M., Vives, L., 2016. Groundwater chemical baseline values to assess the Recovery Plan in the Matanza-Riachuelo River basin, Argentina. Sci. Total Environ. 541, 1516–1530. https://doi.org/10.1016/j.scitotenv.2015.10.006

Zwahlen, F. (ed.), 2004. Vulnerability and risk mapping for the protection of carbonate (karst) aquifers, final report COST Action 620. EUR 20912, European Commission, Brussels, 297 p.

# Supplementary Material

## Subset 1: Hydrochemistry

**Table SM.1.** Summary of the major ions content (median values of time series of the 43 monitored springs for the period September 2013 – October 2015).

| Spring | GU | water-type | Cluster | Cluster Probability (%) | CE (µS/cm) | pH (-) | T (°C) | Ca (meq/L) | Mg (meq/L) | Na (meq/L) | K (meq/L) | $HCO_3$ (meq/L) | Cl (meq/L) | $NO_3$ (meq/L) | $SO_4$ (meq/L) |
|---|---|---|---|---|---|---|---|---|---|---|---|---|---|---|---|
| M-01 | PEm1 | Ca-$HCO_3$ | B | 91.10 | 640.5 | 7.3 | 12.2 | 120.5 | 10.5 | 7.6 | 1.8 | 288.7 | 8.9 | 5.3 | 88.9 |
| M-02 | PEmb | Ca-$SO_4$-$HCO_3$ | B | 100.00 | 493.0 | 7.8 | 10.7 | 78.0 | 13.5 | 4.6 | 1.3 | 141.7 | 4.0 | 3.5 | 133.7 |
| M-03 | PEalb | Ca-$HCO_3$ | A | 100.00 | 306.3 | 7.8 | 11.4 | 61.0 | 2.0 | 2.9 | 1.9 | 184.1 | 2.7 | 2.5 | 4.4 |
| M-04 | POcgs | Ca-$HCO_3$ | A | 100.00 | 470.0 | 7.4 | 10.2 | 95.0 | 6.3 | 2.1 | 2.6 | 289.0 | 3.3 | 3.6 | 15.4 |
| M-05 | Qpe | Ca-$HCO_3$ | A | 100.00 | 307.0 | 7.7 | 10.1 | 66.0 | 1.1 | 2.4 | 0.5 | 190.7 | 2.5 | 2.0 | 3.1 |
| M-06 | Kgp | Ca-$HCO_3$ | A | 100.00 | 251.0 | 8.1 | 7.3 | 54.0 | 5.3 | 3.0 | 0.9 | 166.5 | 3.3 | 2.2 | 9.0 |
| M-07 | POcgs | Ca-$HCO_3$ | A | 100.00 | 461.5 | 7.3 | 9.7 | 101.5 | 4.7 | 3.5 | 0.9 | 296.9 | 3.2 | 2.0 | 12.7 |
| M-08 | Kgp | Ca-$HCO_3$ | A | 100.00 | 384.3 | 7.6 | 5.5 | 87.0 | 4.1 | 3.3 | 1.0 | 269.6 | 3.0 | 1.9 | 9.6 |
| M-09 | Tk | Ca-$SO_4$ | B | 100.00 | $1.2 \cdot 10^3$ | 7.9 | 9.0 | 242.0 | 14.5 | 8.5 | 2.2 | 212.2 | 7.8 | 4.2 | 488.3 |
| M-10 | Tk | Ca-$HCO_3$-$SO_4$ | B | 100.00 | 829.5 | 7.3 | 9.6 | 173.0 | 8.3 | 4.2 | 1.3 | 292.4 | 7.4 | 17.8 | 174.0 |
| M-11 | KMca | Ca-$HCO_3$ | A | 99.93 | 312.0 | 8.0 | 10.7 | 59.5 | 5.6 | 3.7 | 0.7 | 157.5 | 4.2 | 10.9 | 25.3 |
| M-12 | Kgp | Ca-$HCO_3$ | A | 99.99 | 252.0 | 7.9 | 8.5 | 53.5 | 2.3 | 1.7 | 0.6 | 167.3 | 4.3 | 1.9 | 4.1 |
| M-13 | Tm | Ca-$HCO_3$ | B | 96.88 | 574.0 | 7.7 | 11.2 | 96.5 | 19.0 | 9.0 | 1.7 | 253.9 | 20.9 | 1.8 | 97.7 |
| M-14 | PPEc | Ca-$HCO_3$ | A | 100.00 | 190.8 | 8.0 | 5.8 | 39.5 | 1.9 | 1.4 | 0.5 | 118.7 | 2.5 | 3.7 | 2.8 |
| M-15 | PEci | Ca-$HCO_3$ | A | 100.00 | 186.6 | 8.2 | 6.0 | 38.0 | 1.9 | 1.6 | 0.6 | 112.0 | 2.5 | 5.9 | 2.6 |
| M-16 | PEci | Ca-$HCO_3$ | A | 100.00 | 306.0 | 8.0 | 13.4 | 60.0 | 12.0 | 1.0 | 0.8 | 221.0 | 2.5 | 0.0 | 6.3 |
| M-17 | PEci | Ca-$HCO_3$ | A | 100.00 | 361.5 | 8.0 | 7.0 | 67.0 | 14.5 | 1.3 | 1.0 | 251.5 | 2.8 | 7.0 | 3.3 |
| M-18 | PEci | Ca-$HCO_3$ | A | 100.00 | 385.0 | 7.9 | 11.9 | 64.0 | 18.0 | 1.7 | 3.8 | 253.0 | 2.5 | 8.3 | 6.4 |
| M-19 | TJcd | Ca-$HCO_3$ | A | 100.00 | 392.0 | 7.8 | 7.4 | 62.5 | 18.5 | 1.7 | 0.7 | 256.4 | 3.4 | 5.7 | 4.7 |
| M-20 | PEcp2 | Ca-$HCO_3$-Cl | C | 100.00 | 701.6 | 7.7 | 6.2 | 86.0 | 18.0 | 33.0 | 1.1 | 266.9 | 80.9 | 9.1 | 10.7 |
| M-21 | Qcoo | Ca-$SO_4$ | B | 100.00 | 867.3 | 7.4 | 11.8 | 179.5 | 8.6 | 3.3 | 1.2 | 180.4 | 3.8 | 2.0 | 329.7 |
| M-22 | Qvl | Ca-$HCO_3$ | A | 100.00 | 241.0 | 7.9 | 7.4 | 45.0 | 6.2 | 1.6 | 0.4 | 147.4 | 3.6 | 2.7 | 6.5 |
| M-23 | Qt0 | Ca-$HCO_3$ | C | 99.92 | 332.0 | 7.8 | 8.3 | 54.0 | 5.8 | 6.7 | 0.6 | 159.0 | 24.4 | 4.5 | 10.9 |
| M-24 | PPEc | Ca-$HCO_3$ | A | 100.00 | 402.5 | 7.6 | 8.2 | 76.0 | 10.5 | 2.8 | 1.2 | 266.1 | 3.7 | 1.8 | 5.5 |
| M-25 | Kgp | Ca-$HCO_3$ | A | 100.00 | 323.8 | 7.8 | 8.0 | 66.0 | 4.9 | 1.5 | 0.5 | 209.8 | 2.5 | 1.8 | 5.9 |
| M-26 | KMca | Ca-$HCO_3$ | A | 100.00 | 296.3 | 8.1 | 10.5 | 61.0 | 2.4 | 2.6 | 0.5 | 183.5 | 2.7 | 3.0 | 4.9 |
| M-27 | KMca | Ca-$HCO_3$ | C | 100.00 | 492.3 | 7.5 | 9.3 | 90.5 | 2.9 | 11.0 | 0.7 | 241.2 | 39.0 | 3.1 | 9.7 |
| M-28 | Tk | Ca-$SO_4$ | B | 100.00 | $2.1 \cdot 10^3$ | 7.5 | 12.9 | 445.0 | 40.0 | 42.5 | 8.8 | 298.5 | 94.5 | 40.9 | 989.0 |
| M-29 | Qpe | Ca-$HCO_3$ | A | 99.79 | 436.0 | 7.7 | 10.2 | 76.0 | 6.5 | 8.1 | 1.7 | 218.0 | 15.6 | 9.0 | 23.4 |
| M-30 | Tk | Na-Cl | D | 100.00 | $2.5 \cdot 10^5$ | 6.4 | 15.4 | 754.5 | $1.6 \cdot 10^3$ | $1.2 \cdot 10^5$ | $3 \cdot 10^3$ | 249.8 | $1.8 \cdot 10^5$ | 4.4 | $8 \cdot 10^3$ |
| M-31 | PPEc | Ca-$HCO_3$ | A | 100.00 | 353.8 | 7.9 | 8.6 | 75.0 | 4.1 | 1.2 | 0.4 | 234.0 | 2.5 | 2.4 | 4.6 |
| M-32 | POmlg | Ca-$HCO_3$ | A | 100.00 | 461.8 | 7.6 | 10.9 | 94.5 | 1.7 | 3.0 | 0.9 | 201.5 | 6.8 | 60.9 | 20.0 |

| | | | | | | | | | | | | | | | |
|---|---|---|---|---|---|---|---|---|---|---|---|---|---|---|---|
| M-33 | Tk | $Ca\text{-}HCO_3\text{-}SO_4$ | B | 100.00 | 851.0 | 7.1 | 7.8 | 158.5 | 18.5 | 3.8 | 2.2 | 328.8 | 4.6 | 1.7 | 205.9 |
| M-34 | TJb | $Ca\text{-}HCO_3$ | A | 100.00 | 331.8 | 7.6 | 7.6 | 68.5 | 8.4 | 2.8 | 0.7 | 237.0 | 3.5 | 0.9 | 7.3 |
| M-35 | PEcp1 | $Ca\text{-}HCO_3$ | A | 100.00 | 232.0 | 8.1 | 12.6 | 39.5 | 4.6 | 1.5 | 0.4 | 133.7 | 3.2 | 2.9 | 4.1 |
| M-36 | PEmb | $Ca\text{-}SO_4\text{-}HCO_3$ | B | 100.00 | 601.3 | 7.9 | 11.0 | 96.5 | 20.0 | 5.7 | 1.2 | 197.5 | 4.0 | 1.6 | 168.6 |
| M-37 | Qvl | $Ca\text{-}HCO_3$ | A | 99.99 | 223.8 | 8.1 | 8.2 | 45.5 | 2.4 | 2.6 | 0.4 | 133.5 | 4.1 | 3.1 | 4.1 |
| M-38 | Kat | $Ca\text{-}HCO_3$ | A | 99.99 | 486.5 | 7.6 | 8.8 | 86.5 | 15.0 | 2.4 | 0.8 | 303.0 | 3.7 | 0.6 | 22.7 |
| M-39 | POmlg | $Ca\text{-}HCO_3$ | A | 100.00 | 472.3 | 7.5 | 11.2 | 94.5 | 4.2 | 2.4 | 0.5 | 284.5 | 3.0 | 0.6 | 12.8 |
| M-40 | Tk | $Ca\text{-}SO_4$ | B | 100.00 | $1.2\cdot10^3$ | 7.2 | 12.3 | 229.5 | 28.0 | 39.5 | 2.4 | 241.0 | 71.2 | 2.1 | 468.9 |
| M-41 | Tk | Na-Cl | D | 100.00 | $5.7\cdot10^4$ | 7.3 | 12.3 | 550.0 | 76.5 | $1.3\cdot10^4$ | 124.5 | 210.0 | $2.1\cdot10^4$ | 4.9 | $1\cdot10^3$ |
| M-42 | KMca | $Ca\text{-}HCO_3$ | C | 100.00 | 747.0 | 7.5 | 10.6 | 101.5 | 17.5 | 38.0 | 1.0 | 315.3 | 82.3 | 2.2 | 15.3 |
| M-43 | POcgs | $Ca\text{-}HCO_3$ | A | 100.00 | 283.8 | 7.74 | 9.0 | 54.0 | 4.7 | 2.3 | 0.4 | 177.0 | 4.0 | 2.6 | 6.2 |

**Table SM.2.** Average, standard deviation, and coefficient of variation for the time series of solute (CL, $NO_3$ and $SO_4$) concentration in groundwater for the high frequency sampled springs. Besides the same statistics are presented for the spatial distributions of solute concentrations considering the ensemble of the low frequency sampled springs.

| Spring Time Series | Num. Samples | $Cl^-$ | | $NO_3^-$ | | $SO_4^=$ | |
|---|---|---|---|---|---|---|---|
| | | Value[d] | CV | Value[d] | CV | Value[d] | CV |
| M-04[a] | 25 | 4.32±2.43 | 0.56 | 3.88±1.53 | 0.40 | 16.13±2.53 | 0.16 |
| M-22[a] | 25 | 5.35±4.72 | 0.88 | 3.19±2.22 | 0.69 | 7.14±1.90 | 0.27 |
| M-25[a] | 25 | 3.36±1.29 | 0.38 | 2.54±1.54 | 0.61 | 5.87±0.78 | 0.13 |
| M-31[a] | 25 | 4.34±4.00 | 0.92 | 3.03±1.33 | 0.44 | 4.55±0.60 | 0.13 |
| Spring Time Series Avg[b] | | 4.34±3.11 | 0.69 | 3.16±1.66 | 0.53 | 8.42±1.45 | 0.17 |
| Spatial.Avg[c] | | 4.71±2.17 | 0.42 | 6.28±1.80 | 0.41 | 9.10±1.47 | 0.14 |

(a) High frequency sampled spring
(b) Average for the high frequency sampled springs
(c) Spatial average from the low high frequency sampled springs M-03, M-05, M-06, M-07, M-08, M-11, M-12, M-14, M-15, M-16, M-17, M-18, M-19, M-24, M-26, M-29, M-32, M-34, M-35, M-37, M-38, M-39
(d) Average ± Std.Dev

# Subset 2: Exploratory analysis of the original dada

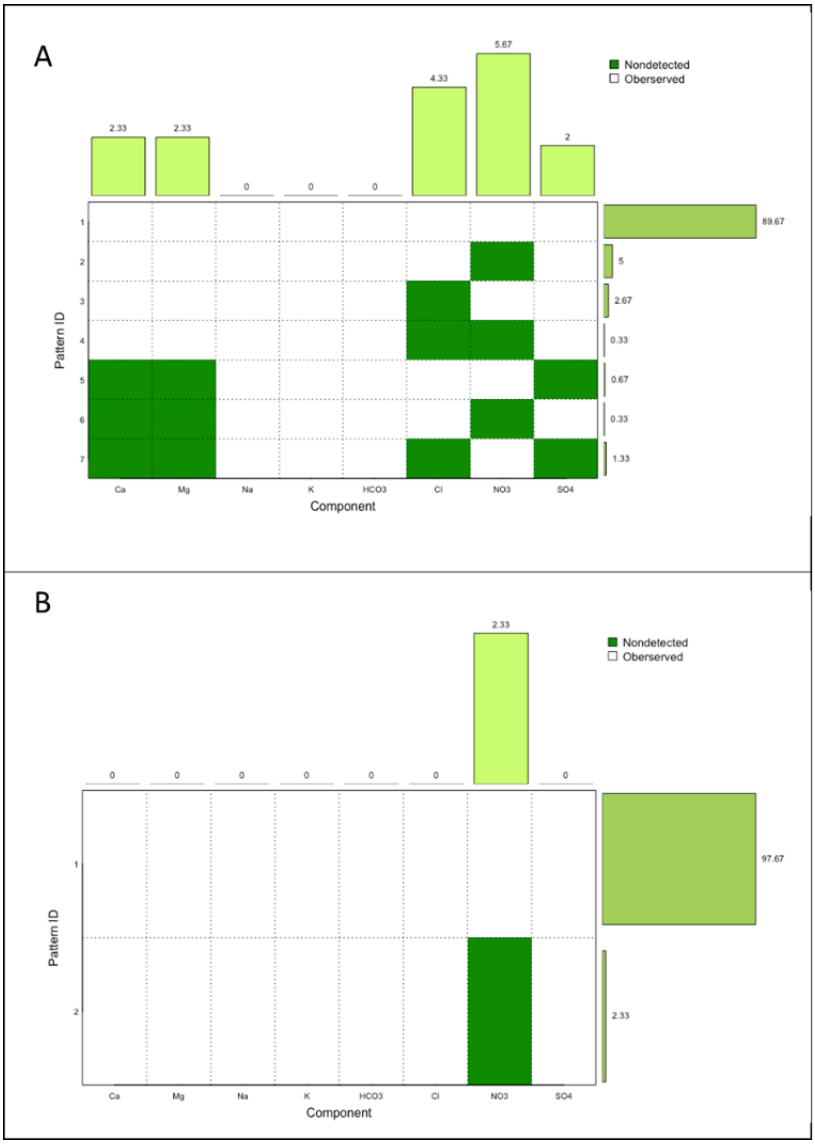


**Fig. SM.2.1.** Pattern diagram of data. The 'zPatterns' function of {zCompositions} package was used for visual exploratory issues and inspecting zero patterns for the data matrix. (A) Data matrix 300 x 8. In this case there are censored values in Cl, NO3, SO4, Ca and Mg ions, most of them related to the 10 snow samples. In total 89,67% of samples have complete value sets. Missing values have been imputed with the 'lrDA' (log ratio Data Argumentation) function (B) Data matrix 43 x 8 (median values).

- **Univariate analysis: Matrix 300 x 8 variables**

Edaplot (combination of histogram, density trace, one-dimensional scattergram and Boxplot in one plot) were calculated for each ion.

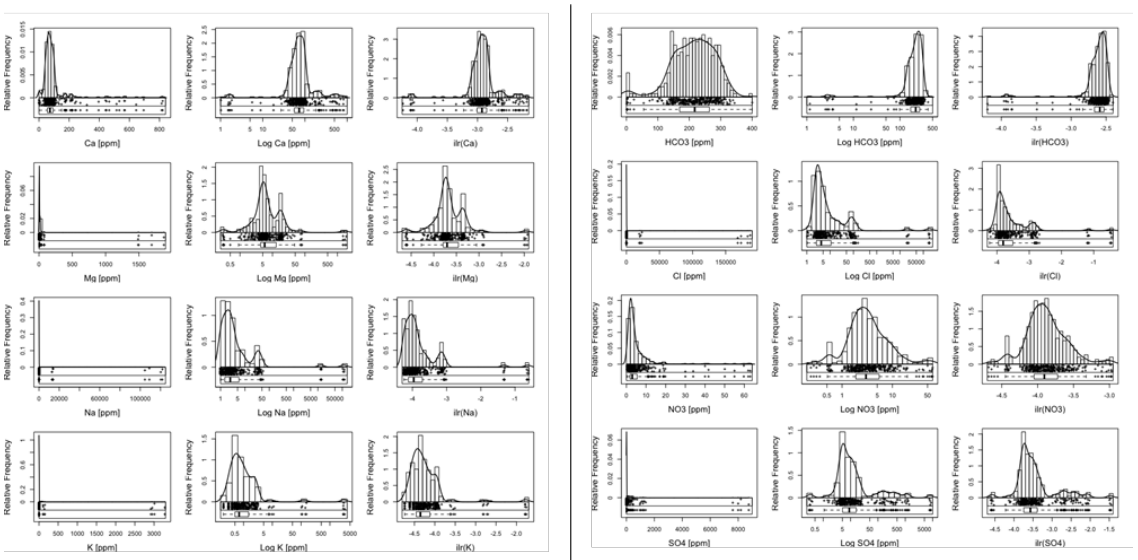


**Fig. SM.2.2.** EDA plot for the eight ions (matrix 300x8)

# Subset 3: Principal Component Analysis

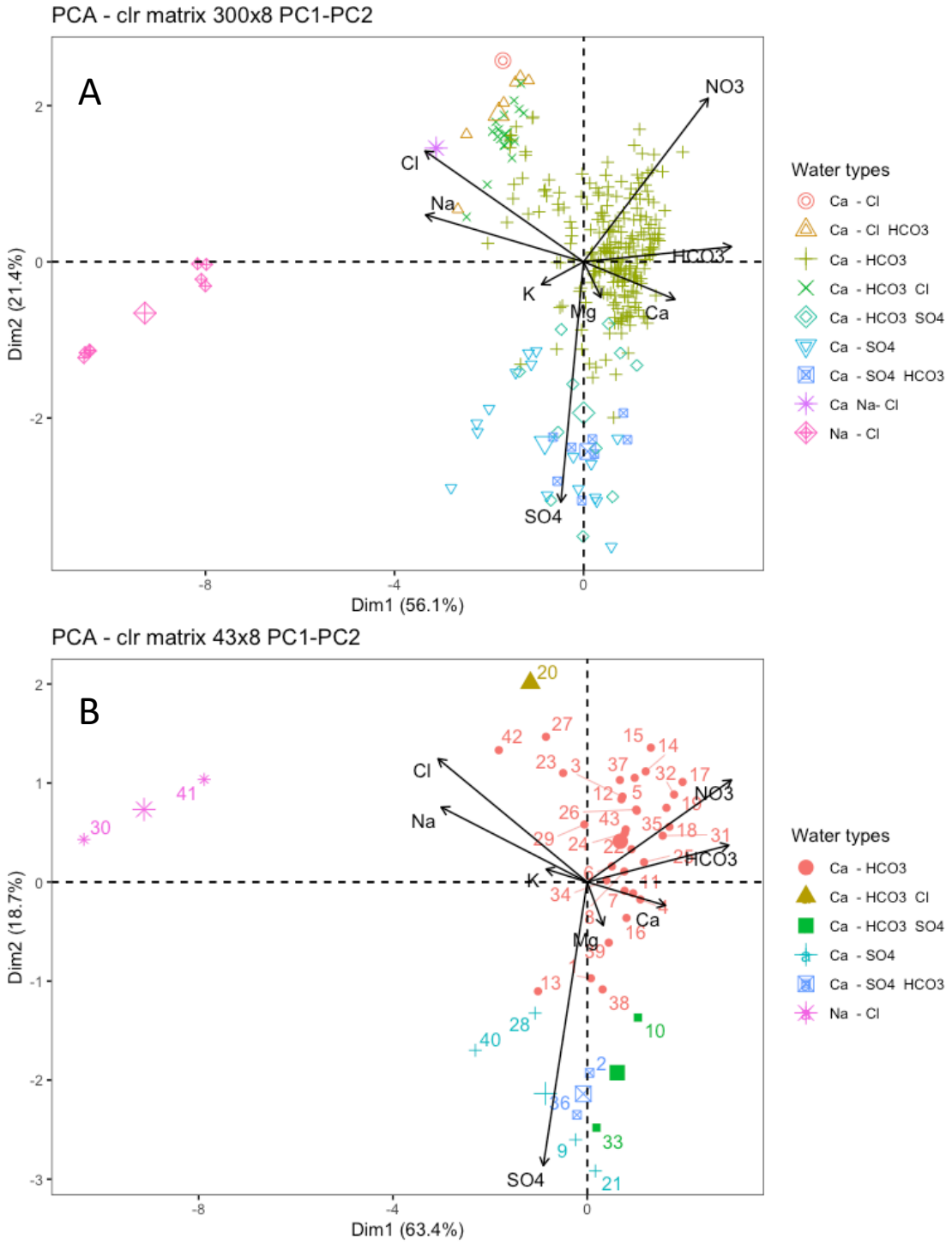


**Fig. SM.3.1.** Biplots clr-transformed, PC1-PC2 with the links interpreted for the data Matrix 300x8 (A) and the data Matrix 43x8 (B)

**Table SM.3.1** Parameters 'included' and 'excluded' for the MSA.

| Parameters 'included' | |
|---|---|
| Major ions | Ca, Mg, Na, K, HCO3, Cl, NO3, SO4 |
| (8 variables) | Existence of left-censored values in the Compositional Data set (no missing values): |
| Matrix 300x8 and Matrix 43x8 | Ca: 2% samples < LOQ (samples of snow) [<2ppm]) |
| | Mg: 2% samples < LOQ (samples of snow) [<0,4ppm]) |
| | SO4: 2% samples < LOQ (samples of snow) [<0,7ppm]) |
| | Cl: 3% (springs samples) + 1,3% (snow samples) < LOQ [<2,5ppm]) |
| | NO3: 1 sample with a value below LOQ [<1ppm]) (spring sample) |
| **Parameters 'excluded'** | |
| EC, TDS, pH, Eh | Parameters with additive characteristics. |
| | Non-compositional data |
| T° | Physical parameter. Non-compositional data |
| F-; CO3-; | >90% samples < LOQ - (*) severe degree of censored data |
| DOC | >28% samples < LOQ |
| NH4 | >67% samples < LOQ - (*) high degree of censored data |
| Isotopes | Not considered although there are some references (Tolosana-Delgado, 2005; Puig et al 2011) |
| Total alkalinity | Parameter linked to HCO3 concentration |
| DUR (water hardness) | Parameter linked to Ca and Mg concentration |

# Subset 4: Model-based clustering results

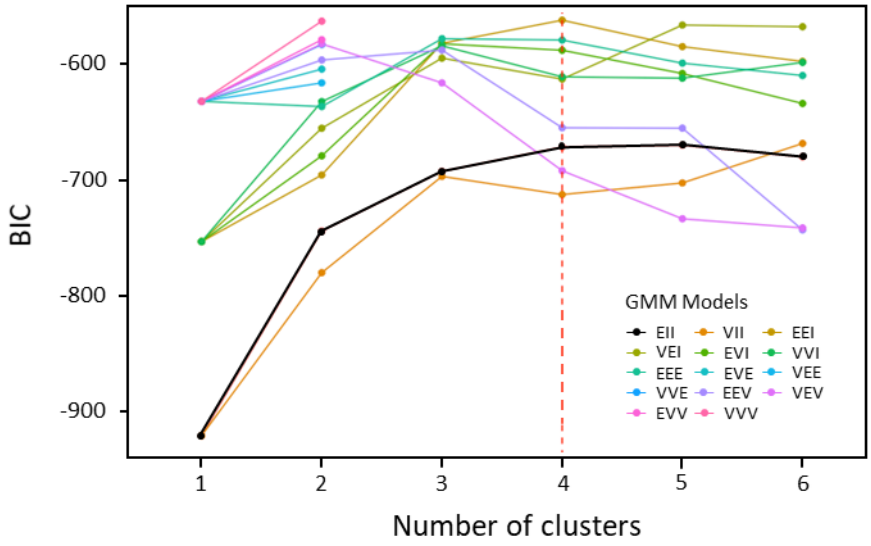


**Fig. SM.4.1.** Graphic of the BIC criteria for the considered 14 GMM models. The lowest BIC value can be observed considering the 'EEI' model and 4 clusters. (See Scrucca et al., 2016; for the corresponding geometric characteristics of the EEI model)

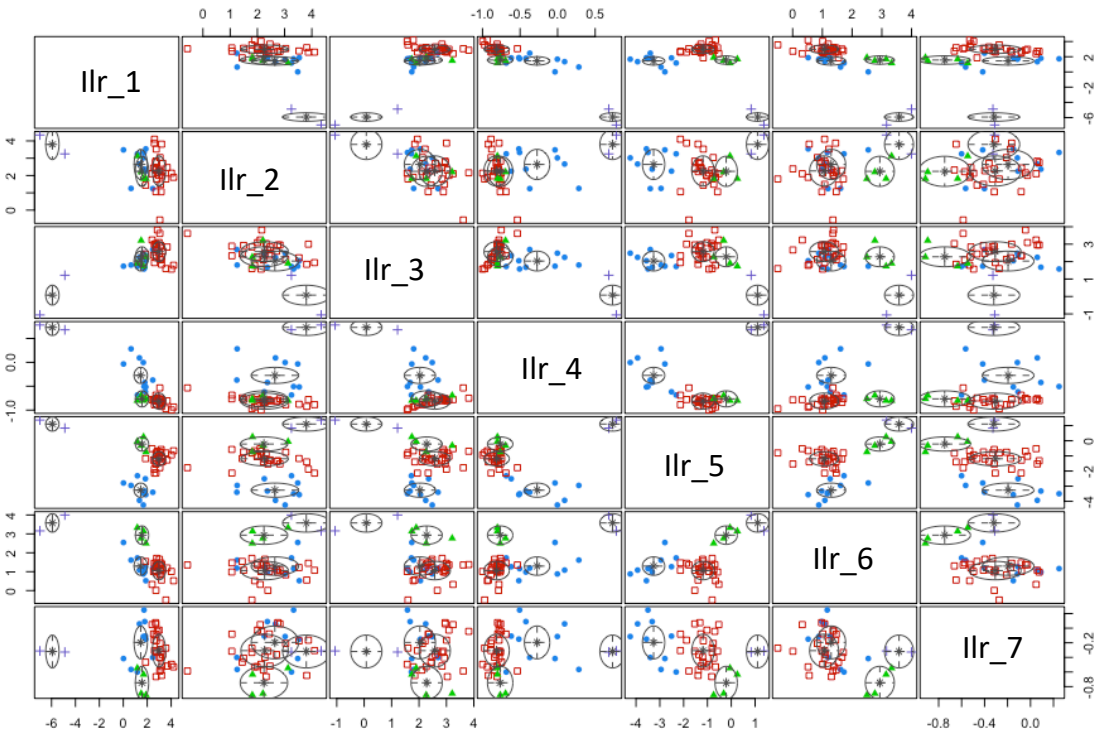

**Fig. SM.4.2.** Scatterplot matrix obtained with the model-based clustering process using the dataset Matrix (43x8) and seven ilr balances (D-1, being D the dimension of the matrix)

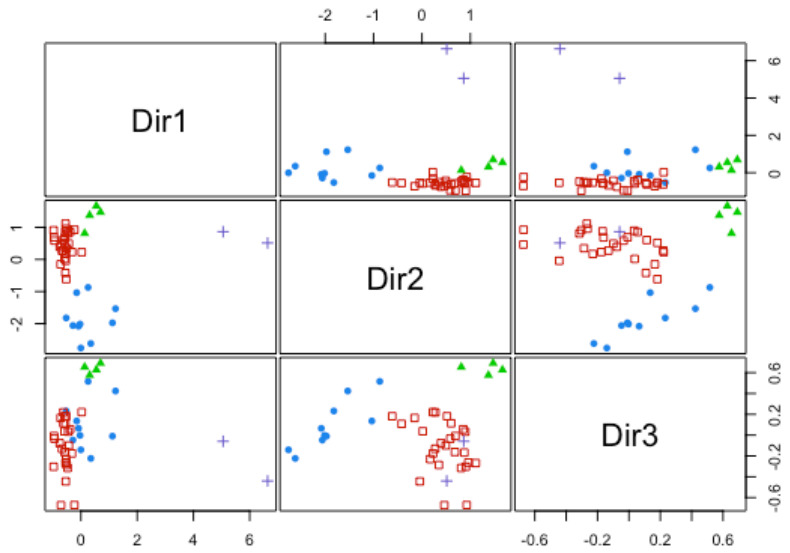


**Fig. SM.4.3.** scatterplot of the reduced ilr-matrix

**Table. SM.4.1.** Calculated principal dimension of the reduced ilr-matrix.

| | **Dir1** | **Dir2** | **Dir3** |
|---|---|---|---|
| ilr_1 | -0.456 | 0.166 | -0.075 |
| ilr_2 | 0.007 | 0.094 | -0.062 |
| ilr_3 | -0.183 | 0.197 | -0.028 |
| ilr_4 | **0.836** | -0.252 | -0.802 |
| ilr_5 | 0.242 | **0.913** | -0.231 |
| ilr_6 | 0.013 | 0.145 | 0.387 |
| ilr_7 | 0.037 | -0.083 | -0.378 |

**Table SM.4.2.** Mean groundwater chemistry of the spring water groups determined from the model-based clustering with GMM (model 'EEI' and k=4 clusters)

| | Cluster A | | | Cluster B | | | Cluster C | | | Cluster D | | |
|---|---|---|---|---|---|---|---|---|---|---|---|---|
| | Avg. | Max. | Min. | Avg. | Max. | Min. | Avg. | Max. | Min. | Avg. | Max. | Min. |
| CE (µS/cm) | 337 | 486 | 186 | 875 | 2102 | 493 | 568 | 747 | 332 | 152135 | 247100 | 57170 |
| pH (-) | 7.8 | 8.2 | 7.3 | 7.5 | 7.9 | 7.1 | 7.6 | 7.8 | 7.5 | 6.9 | 7.3 | 6.4 |
| T (°C) | 9.1 | 13.0 | 5.5 | 10.9 | 12.9 | 7.8 | 8.6 | 10.6 | 6.2 | 13.9 | 15.4 | 12.3 |
| Ca (mg/L) | 66.3 | 101.5 | 38.0 | 181.9 | 445.0 | 78.0 | 83.0 | 101.5 | 54.0 | 652.3 | 754.5 | 550.0 |
| Ca (mg/L) | 6.4 | 18.5 | 1.1 | 18.1 | 40.0 | 8.3 | 11.1 | 18.0 | 2.9 | 835.3 | 1594.0 | 76.5 |
| Mg (mg/L) | 2.4 | 8.1 | 1.0 | 12.9 | 42.5 | 3.3 | 22.1 | 38.0 | 6.7 | 63938.8 | 114650.0 | 13227.5 |
| Na (mg/L) | 0.9 | 3.8 | 0.4 | 2.4 | 8.8 | 1.2 | 0.8 | 1.1 | 0.6 | 1553.5 | 2982.5 | 124.5 |
| K (mg/L) | 209.7 | 303.0 | 112.0 | 243.5 | 328.8 | 141.7 | 245.6 | 315.3 | 159.0 | 229.9 | 249.8 | 210.0 |
| $HCO_3$ (mg/L) | 3.8 | 15.6 | 2.5 | 22.7 | 94.5 | 3.8 | 56.7 | 82.3 | 24.4 | 99596.0 | 178185.5 | 21006.4 |
| $NO_3$ (mg/L) | 5.5 | 60.9 | 0.6 | 8.1 | 40.9 | 1.6 | 4.7 | 9.1 | 2.2 | 4.6 | 4.9 | 4.4 |
| $SO_4$ (mg/L) | 8.8 | 25.3 | 2.6 | 314.5 | 989.0 | 88.9 | 11.6 | 15.3 | 9.7 | 4667.8 | 8093 | 1242.6 |

**Table SM.4.3.** Conditional probabilities (P) of belonging to a certain cluster obtained in the model-based clustering analysis using a GMM ('EEI' model, k = 4). The springs belonging to an unique cluster (i.e. P=1) are highlighted in blue

| | Probability of belonging to a certain cluster | | | | | | | | |
|---|---|---|---|---|---|---|---|---|---|
| **Spring** | Cluster-A | Cluster-B | Cluster-C | Cluster-D | **Spring** | Cluster-A | Cluster-B | Cluster-C | Cluster-D |
| M-01 | 0.089 | 0.911 | 0 | 0 | M-23 | 0.001 | 0 | 0.999 | 0 |
| M-02 | 0 | **1** | 0 | 0 | M-24 | **1** | 0 | 0 | 0 |
| M-03 | **1** | 0 | 0 | 0 | M-25 | **1** | 0 | 0 | 0 |
| M-04 | **1** | 0 | 0 | 0 | M-26 | **1** | 0 | 0 | 0 |
| M-05 | **1** | 0 | 0 | 0 | M-27 | 0 | 0 | **1** | 0 |
| M-06 | **1** | 0 | 0 | 0 | M-28 | 0 | **1** | 0 | 0 |
| M-07 | **1** | 0 | 0 | 0 | M-29 | 0.998 | 0 | 0.002 | 0 |
| M-08 | **1** | 0 | 0 | 0 | M-30 | 0 | 0 | 0 | 1 |
| M-09 | 0 | **1** | 0 | 0 | M-31 | **1** | 0 | 0 | 0 |
| M-10 | 0 | **1** | 0 | 0 | M-32 | **1** | 0 | 0 | 0 |
| M-11 | 0.999 | 0.001 | 0 | 0 | M-33 | 0 | **1** | **1** | 0 |
| M-12 | **1** | 0 | 0 | 0 | M-34 | **1** | 0 | 0 | 0 |
| M-13 | 0.031 | 0.9687 | 0.0003 | 0 | M-35 | **1** | 0 | 0 | 0 |
| M-14 | **1** | 0 | 0 | 0 | M-36 | 0 | **1** | 0 | 0 |
| M-15 | **1** | 0 | 0 | 0 | M-37 | 0.9999 | 0 | 0.0001 | 0 |
| M-16 | **1** | 0 | 0 | 0 | M-38 | 0.9999 | 0.0001 | 0 | 0 |
| M-17 | **1** | 0 | 0 | 0 | M-39 | **1** | 0 | 0 | 0 |
| M-18 | **1** | 0 | 0 | 0 | M-40 | 0 | **1** | 0 | 0 |
| M-19 | **1** | 0 | 0 | 0 | M-41 | 0 | 0 | 0 | **1** |
| M-20 | 0 | 0 | **1** | 0 | M-42 | 0 | 0 | **1** | 0 |
| M-21 | 0 | **1** | 0 | 0 | M-43 | **1** | 0 | 0 | 0 |
| M-22 | **1** | 0 | 0 | 0 | | | | | |

# Subset 5: CoDa approach vs classical standardization (z-score method)

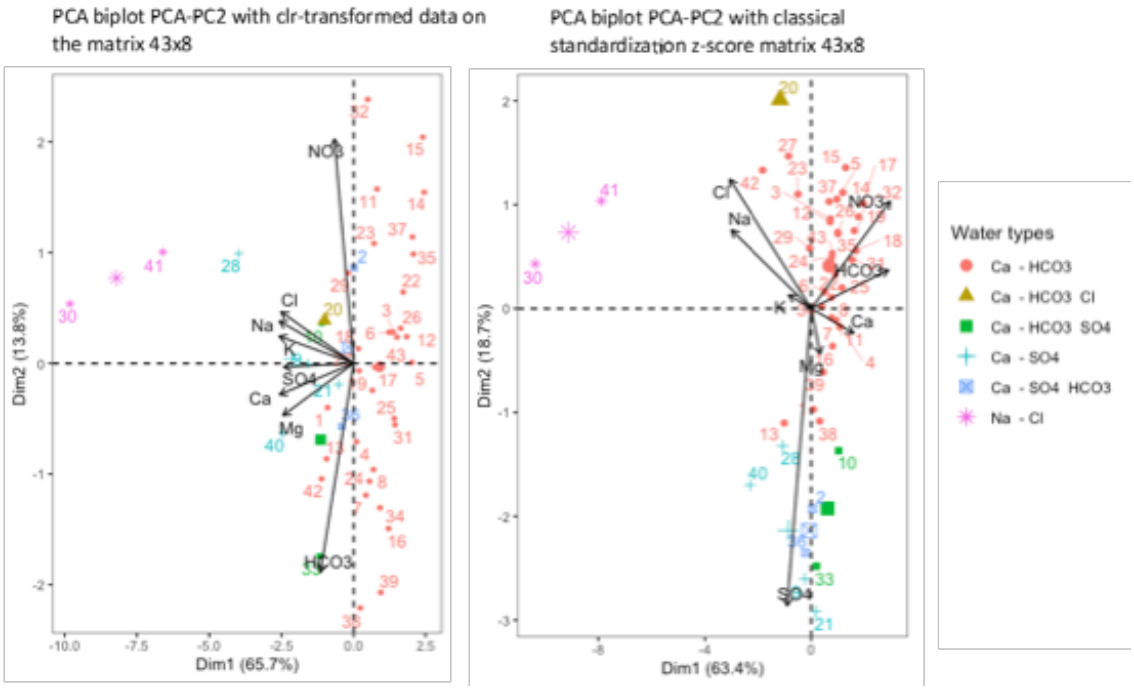


**Fig. SM.5.1.** Biplot considering the classical standardization z-score approach (A) vs. considering the CoDA approach (B) on the dataset Matrix (43x8). As can be shown, considering the effect of the closed nature of geochemical data (CoDA approach) has a critical effect on the variable loading's distribution into the biplot, and no sense variable loading results are obtained when the classical standardization z-score approach is assumed.

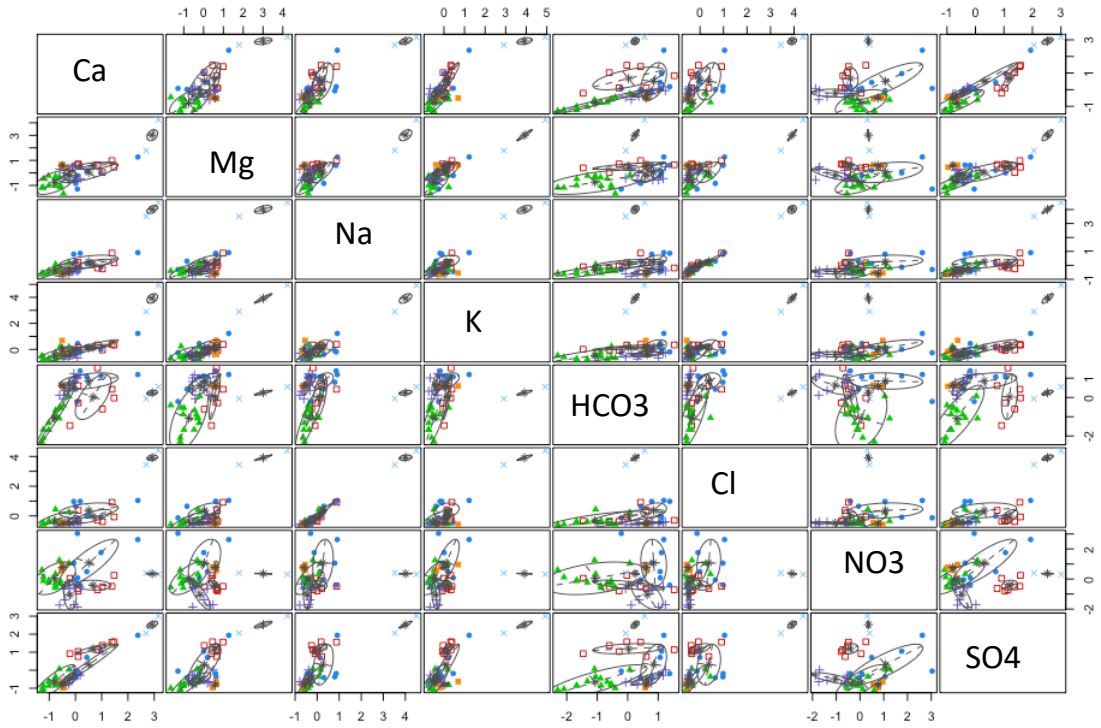


**Fig. SM.5.2.** Scatterplot matrix obtained with the model-based clustering process using transformed data form the dataset matrix (43x8) and using the classical standardization z-score approach.

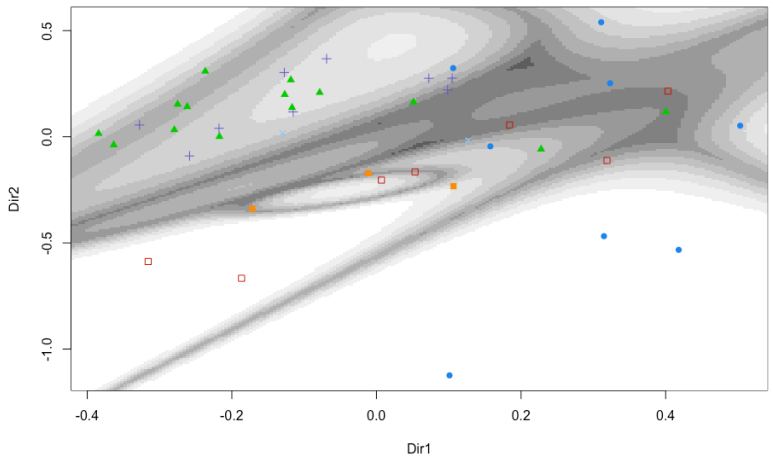


**Fig. A.5.3.** Density biplot for PC1 vs PC2 components obtained from GMM for the Matrix (43x8) of data z-score transformed after dimension reduction.

## Subset 6: Preliminary clustering analysis considering 'hard' clustering methods

Clustering is an unsupervised classification method widely used in hydrogeological research studies. There are multiple and variate "hard" clustering (where each data point can only belong to exactly one cluster; as e.g. the agglomerative hierarchical clustering HCA; and the partitional methods such as the k-means, k-medoids, among others) and criteria to take into account. The hierarchical clustering is a set of nested clusters that are organized as a tree (dendogram). The partitional clustering look for a division of the set of data objects into non-overlapping subsets (clusters) such that each data object is in exactly one subset. The selection of the method for clustering, the assumed number of clusters (to be used as initial centroids in case of the partitional methods), and the dissimilarity and linkage method selected have a strong impact on the clustering results obtained. Therefore, their use relies heavily on the analyst's knowledge to classify the clusters in a meaningful way. In practice it's important to test different methods, test the different indexes that allows found the best one, but finally take a look for the one with the most hydrogeological sense and the most useful or interpretable solution.

The clValid() function of the {clValid} R package (Brock et al. 2008), calculates validation measures for a given set of clustering algorithms and number of clusters. Available options are "hierarchical", "kmeans", "diana", "fanny", "som", "model", "sota", "pam", "clara", and "agnes", with multiple choices allowed. The internal measures include the connectivity, the silhouette coefficient and the Dunn index.

The fviz_nbclust() function of the {factoextra}R package (Kassambara and Mundt, 2016) determines and visualize the optimal number of clusters using computing the three different methods [elbow, silhouette and gap statistic]. Allowed methods include: partitional clustering "kmeans", "k-medoids" (pam, clara), "funny" (fuzzy clustering methods), etc.

The NbClust() function of the {NbClust} R package (Charrad et al. 2014) provides 30 indices for determining the relevant number of clusters and proposes to users the best clustering scheme from the different results obtained by varying all combinations of

number of clusters, distance measures, and clustering methods. The results can be visualized in a summary graph.

In order to inspect the suitability of considering 'hard' clustering methods to determine the optimal number of clusters (k), a first and preliminary analysis was performed using the clValid(), fviz_nbclust() and NbClust() functions using ilr coordinates with the Matrix 43x8. The clustering models may account for different linkage methods (i.e., '*complete*', '*average*', 'single' and '*ward*') and dissimilarity metrics ('*Euclidean*' and '*Manhattan*', among others). Results are presented in Fig. A.6.1., Fig. A.6.2. Fig. A.6.3.

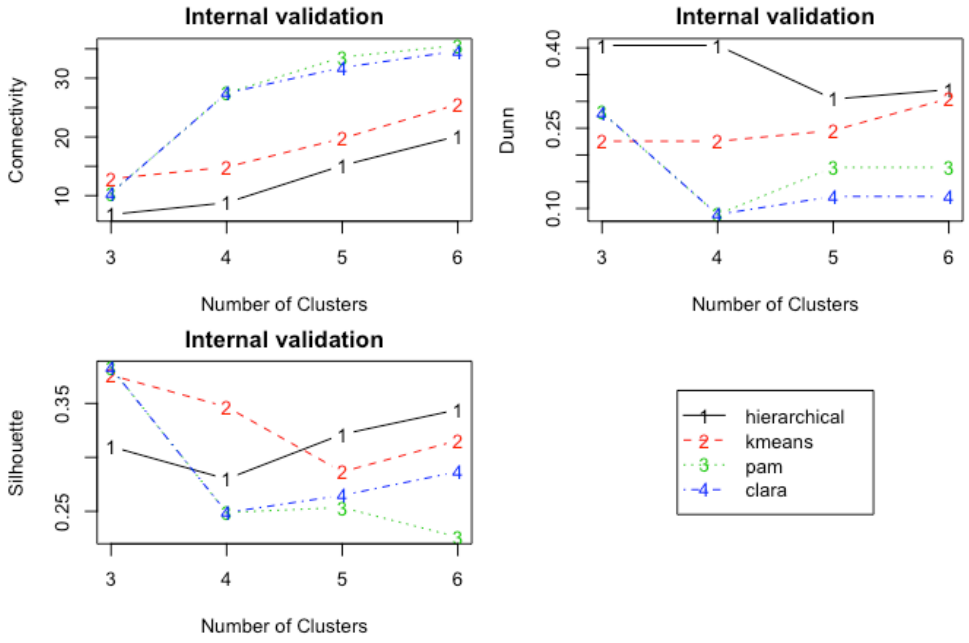


**Fig. A.6.1.** Measures of connectivity, the silhouette coefficient and the Dunn indexes obtained using the function clValid()

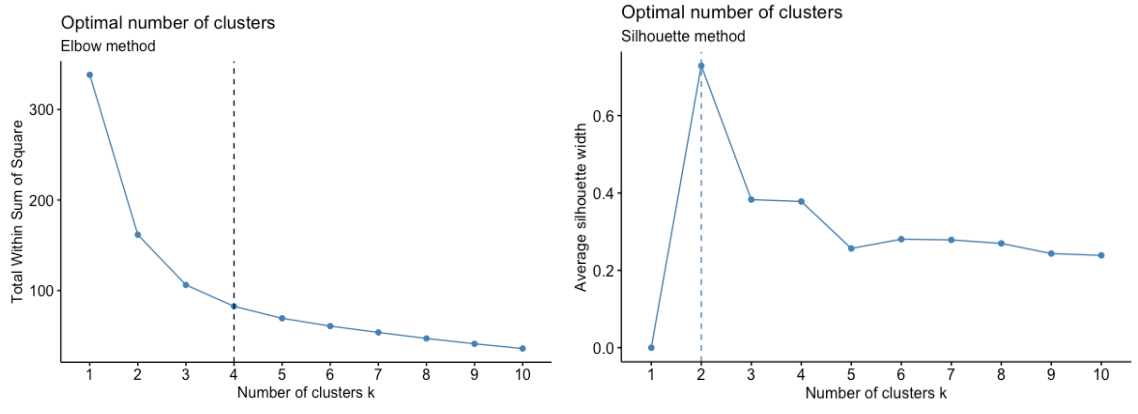

**Fig. A.6.2.** Results of the Elbow and Silhouette methods using the fviz_nbclust() function

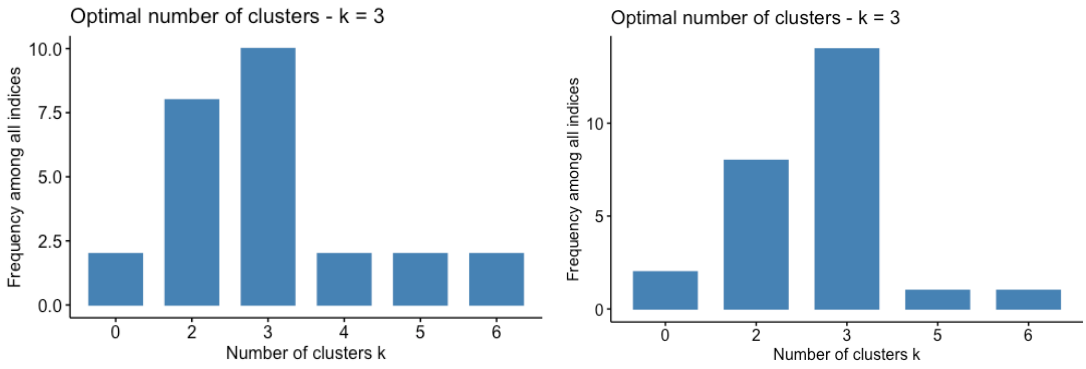


**Fig. A.6.3.** Results obtained using NbClust() function for different cluster agglomeration methods: linkage 'ward.D' and 'complete'; distance = "euclidean".

The results obtained with the function clValid() suggest that the best number of cluster k is 3 but with no clear clustering method prevailing to the others. The results obtained with the Elbow method using the fviz_nbclust() function shows suggests that the best k value would be 4, whereas in the Silhouette method using the same function suggest that the best k value would be 4. The results obtained using NbClust() function for different cluster agglomeration methods: linkage 'ward.D' and 'complete' suggest that the best number is 3.

In summary, the results obtained indicates that good models would be obtained using *hierarchical* and *k-medoids* methods and for k clusters between 2 and 4. So there is no definitive and clear answer to the question about what which would be best method and the best number of k. Therefore it is concluded that the optimal number of clusters is somehow subjective and depends on the method used for measuring similarities and the parameters used for partitioning but also the criteria used to selected them, which cause that it is not evident to determine which could be the best grouping model for the available data using 'hard' clustering methods.